



Harvesting Energy from Decelerating Vehicles

A Major Qualifying Project

Submitted to the Faculty of

WORCESTER POLYTECHNIC INSTITUTE

In partial fulfillment of the requirements for the

Degree of Bachelor Science

In Mechanical Engineer and Electrical and Computer Engineering

By:

Kurt J Bilis

Mary Ellen B Osler

Samuel N Smith

Date: 3/23/2018

Approved by:

John Sullivan

Alexander Emanuel

Abstract

In this project we designed and created a prototype capable of harvesting kinetic energy normally converted to heat by vehicles during braking and converted it to electrical energy to be used to power nearby streetlights. A slider crank mechanism converted linear motion to radial motion and a permanent magnet generator that we designed and prototyped created a system to accomplish this energy harvest. The system was designed to have minimal impact on vehicle operators and/or passengers.

Acknowledgements

We would like to thank our advisor, Professor Sullivan for his guidance and advice throughout our design process. We would also like to thank our co-advisor, Professor Emanuel for his advice on the electrical component of this project. We express gratitude towards the Mechanical Engineering and Electrical and Computer Engineering departments of WPI for allowing us to use their facilities and for ordering parts for the prototype.

List of Tables

Table 1: Inertia study for full-scale ramp	40
Table 2: Inertia study for the prototype model ramp	43

List of Figures

Figure 1: Completed prototype	1
Figure 2: Piezoelectric device.....	4
Figure 3: Map of daily traffic through Worcester County [5]	5
Figure 4: Comparison of power efficiency between HPS and LED street lights [2].....	7
Figure 5: Current generated by an armature from two angles [20].....	8
Figure 6: Diagram of a PMG [12].....	9
Figure 7: Speed bump vs. speed hump [6].....	10
Figure 8: Springboard design.....	11
Figure 9: Rack and pinion.....	12
Figure 10: Before the ramp.....	13
Figure 11: Beginning of ramp.....	13
Figure 12: Just before the end of the ramp	13
Figure 13: Static ramp design	14
Figure 14: Conservation of energy equation.....	14
Figure 15: Behavior alongside a static ramp.....	15
Figure 16: Ramp with a spring on the end.....	15
Figure 17: FBD of ramp treated a cantilever beam.....	16
Figure 18: Theta approximation justification	16
Figure 19: New reaction at the spring.....	16
Figure 20: Equation B, solving for db	17
Figure 21: Equation solved in terms of $d\theta$	17
Figure 22: Instantaneous angle vs. instantaneous position	17
Figure 23: Behavior along a dynamic ramp.....	18
Figure 24: Torque	18
Figure 25: Derivation for inertia.....	19
Figure 26: Angular velocity equation	20
Figure 27: Faraday's law for voltage induced in a coil	21
Figure 28: Dimensions of a multilayer coil [20].....	22
Figure 29: RPM equation.....	23

Figure 30: First generation coil.....	23
Figure 31: Second generation coil	24
Figure 32: Formula for intersection between two circles	25
Figure 33: Intersecting circles' connecting area.....	26
Figure 34: Formulas to calculate x and y.....	26
Figure 35: Results of code ran at 60 RPM.....	27
Figure 36: Saturated steel (left) vs. unsaturated steel (right)	28
Figure 37: Diagram of generator design (measurements in inches)	29
Figure 38: Coil test, core vs coreless	30
Figure 39: Multisim circuit	31
Figure 40: Multisim circuit LED voltage.....	32
Figure 41: Schematic for prototype generator (coreless) output	32
Figure 42: Generator wheel design.....	33
Figure 43: Esprit code for the generator wheel.....	34
Figure 44: Esprit file for stationary generator wheel	35
Figure 45: Stationary generator wheel.....	35
Figure 46: Ramp location.....	36
Figure 47: Full length crankshaft requirement.....	37
Figure 48: Torque limiter.....	38
Figure 49: One-way clutch mechanism	38
Figure 50: Simplified early CAD model (left) Final CAD model (right).....	41
Figure 51: Acrylic ramp with vinyl logo	42
Figure 52: Output voltage of 4 coils in series	46
Figure 53: Completed prototype	47
Figure 54: Connecting arm	48
Figure 55: New slider crank.....	48
Figure 56: Output from generator powered by hand	50
Figure 57: Voltage across resistor when drill powered	51
Figure 58: Output circuit of generator	52

Table of Contents

Acknowledgements	ii
List of Tables	iii
List of Figures	iv
Table of Contents	vi
Chapter 1. Introduction	2
Chapter 2. Background	3
2.1 Green devices	3
2.2 Traffic patterns	4
2.3 Street lights	6
2.4 Generator	7
2.4.1 Alternator	7
2.5 Speed bumps	9
Chapter 3. Design model	11
Chapter 4. Methodology	21
4.1 Coil Design	21
4.1.1 Coil dimensions	21
4.2 Intersection area	25
4.3 Steel Saturation	27
4.4 Generator Design	28
4.5 Drill test	29
4.6 Output Circuit Design	31
4.7 Machining	33
4.8 Inertia calculations	36

4.9 Torque Estimation	44
4.9.1 Finding Torque Experimentally	45
4.9.2 Removing Steel Cores	46
4.10 Ramp prototype construction	47
Chapter 5. Results	50
Chapter 6. Conclusions	53
References	54
Appendix A: Car Weights	57
Appendix B: MATLAB Code	58
Appendix C: Pendulum test results	61
Appendix D: Intersection calculator code	63
Appendix E: Single Coil Drill Test	66
Appendix F: Four Coil Drill Test	67

Executive Summary

The premise for our design is a mechanism that aids in the deceleration of a vehicle, creating useful energy which ultimately lessens the wasted heat that is generated by the brakes. Using a series of cranks, gears, and springs our mechanism slows the car down, minimizing wear on the brakes while at the same time powering a generator which produces electrical energy. This electrical energy is used to power a series of LED streetlights, which run on less energy than traditional metal-halide lights and increase road safety by providing brighter light for drivers to see by.

After reviewing the mechanisms which were available for completing this task we decided to create a ramp which actuates a slider crank mechanism in order to turn a magnet disc for a generator. This selection is beneficial due to it having a low number of moving parts in order for the mechanism to provide simple and consistent output to power nearby streetlights. The use of one way clutches in our system also allows for one actuation of the ramp to provide several rotations of the output shaft resulting in more power overall.

We created models of the physical situation that takes place as a vehicle passes over the system and with the research we conducted parameters were selected that allow for the system to be non-intrusive to passengers in the vehicles.

Our research and prototyping of a system capable of accomplishing this task resulted in a ramp that is capable of illuminating an array of LEDs when a load is applied to the ramp. The generator produced 4.2 volts AC for a magnet disc that rotates around 100 RPM. Pictured below in Figure 1 is the final prototype.

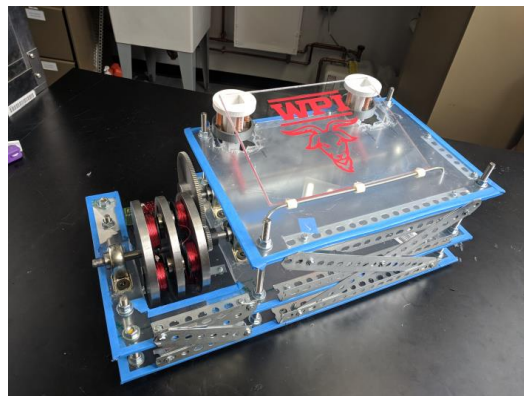


Figure 1: Completed prototype

Chapter 1. Introduction

Everyday thousands of Americans use freeways as their main thoroughfares to get to their final destinations due to their high travel speeds and convenience. However, in order to reach the exact address, drivers also need to use secondary roads. Off-ramps connect the high-speed freeways to the more relaxed secondary roads. As the car slows down on the off-ramp, the brakes heat up due to the friction force that is applied by the brake pads onto the calipers. This friction generates waste heat which is not usable by the vehicle and is ultimately lost to the atmosphere.

The premise for our design is a mechanism that aids in the deceleration of a vehicle, creating useful energy which ultimately lessens the waste heat that is generated. Using a series of cranks, gears, and springs our mechanism slows the car down reducing wear on the brakes while at the same time powering a generator which produces electrical energy. The electrical energy produced would be used to power a series of LED streetlights, which run on less energy than traditional metal-halide lights and provide brighter light for drivers' visibility. The new LED lights would improve the safety of the freeways and off-ramps for drivers and drivers will have to change their brakes less frequently due to less wear.

Chapter 2. Background

To create develop our mechanism, the team researched technologies already in use, traffic on off-ramps, and street light power consumption.

2.1 Green devices

To understand the market space for our device we searched for competitors who had created similar products. From our research we found two similar designs which are the Electro-Kinetic Road Ramp made by Highway Energy Services Ltd. and a patent for an Electric Power Generating Speed Bump by Victor Dmitriev.

The electro-kinetic ramp uses a flywheel that spins when cars drive over it. The inertia of the spinning flywheel rotates a generator which produces electrical power [27]. The system would store this energy in batteries and feeds the excess energy back into the power grid. This energy can be used to power street or traffic lights which improves safety by increasing visibility and making intersections safer for drivers. The company estimates that the ramp can produce between 5 and 50 kWh of power under normal traffic conditions. However, the estimated cost of building and installing one of these systems is \$23,000 [27]. Some other downsides to the high entry cost of this design include the fact that it is built on a flat roadway, which means cars need to expend extra energy, and therefore gas, to get over it. Consequently, the energy that is produced by this design is not free due to the drivers needing to use more gas to make it over the mechanism.

The next design is a patent by Victor Dmitriev. This patent modeled a device shaped like a normal speed bump that would compress when cars drove over the top. This compression would drive a linear electric generator inside of the speed bump to generate electricity [9]. However, this design had the same flaw as the above design of the electro-kinetic ramp because it still required cars to put in extra energy into moving over the device.

Another green technology that harvests energy from roads ditches the mechanical components in favor of piezoelectrics as a means for generating electricity. Piezoelectrics work by applying stress, strain, or pressure to crystalline materials in order to get an output as seen below in Figure 2 [18]:

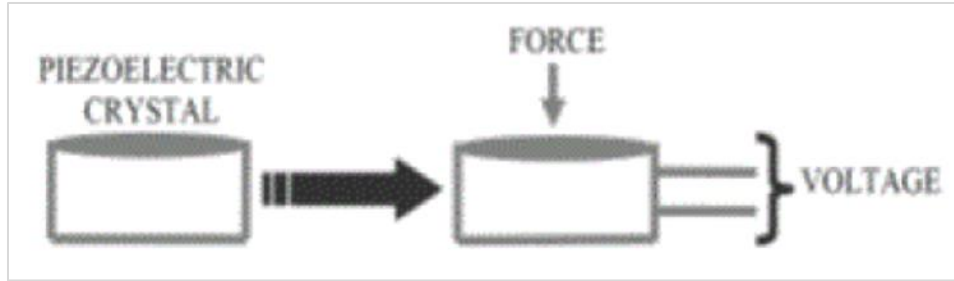


Figure 2: Piezoelectric device

Two researches, Kour and Charif, write an article on the application of piezoelectric devices in roadways to harvest energy. They found their results were satisfactory in providing 0.3 kW per car that travels one kilometer on a single lane piezoelectric roadway [18]. However piezoelectric materials are fairly new and difficult to implement into current roadways since there are no regulations in their production.

These competitors showed us a goal that we wanted to achieve which was to be able to create a device that was able to create a steady and renewable source of energy. These competitors illuminated the possibility of powering the immediate surroundings as well as a possible way to feed power back to the communities our device is installed in. They also illuminated shortcomings of these devices which included that their placement on flat surfaces requires greater energy output by a car instead of lessening brake wear and waste heat.

2.2 Traffic patterns

It was important for our group to note the volume of traffic on freeways to see if a device placed on an off-ramp would be a feasible location to gather energy. In Massachusetts specifically, we can observe the average daily traffic numbers with an online tool provided by the Central Transportation Planning Staff (CTPS) along with Figure 3.

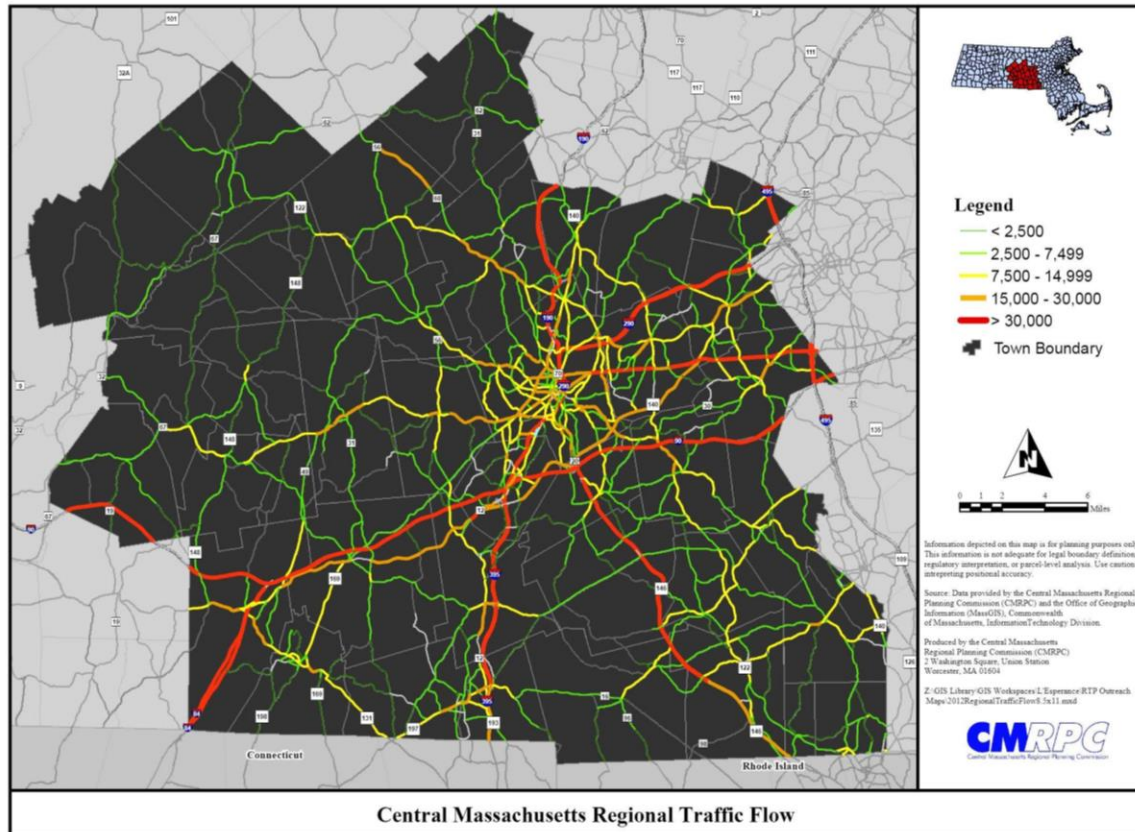


Figure 3: Map of daily traffic through Worcester County [5]

Variations occur at different locations in the state, but interstate 395 near Worcester, Massachusetts sees over 30,000 cars daily. The Massachusetts Turnpike sees over 90,000 cars passing through Worcester County daily [3]. Interstate 290 is also among these roads seeing high traffic volumes daily, 100,000 vehicles according to the CTPS tool. Since there are ten exits off of interstate 290 that pass through Worcester, our group assumed that a typical off-ramp could see around 3,000 vehicles per day, with the possibility of up to 10,000. This data gave our group a good indication for the traffic that could be anticipated if our system was installed on these off ramps.

It is also important to observe what kinds of cars are actually using the freeways in Massachusetts. There are different classes of vehicles based on the wheelbase and weight they have. We broke the many different classes of vehicles into three different classes for simplicity: two-wheeled vehicles, four-wheeled vehicles, and more than four-wheeled vehicles [23]. Four-wheeled vehicles are the biggest class due to the fact that they are the majority of automobiles that use freeways. In fact, this class makes up about 71% the total amount of vehicles [25]. There

is also the greatest variation on weights for this four-wheeled class. Weights can range from as low as 1,800 pounds to over 5,000 pounds [23]. A list of common vehicles and their weights is in Appendix A. The average weights for two-wheeled and more than four-wheeled vehicles are 450 and 3300 lbs respectively. However, semi-trailer trucks can weigh greater than 30,000 lbs [23]. Understanding the weights of different vehicles is vital to having the ability to predict the amount of energy available for harvesting. The weight of a vehicle determines how quickly and with how much force it will depress our device. Our generator has a desired rate of rotation and knowing the range of weights was important for us to create a device that ensures that no matter what vehicle is using the device, we are still spinning our generator at the proper rate.

2.3 Street lights

Drivers are less likely to cause accidents at night when a street is well lit. However, street lights require power, which means they cannot be used if they are placed in a location without access to the power grid. Our device would enable streetlights to be placed next to any section of road without needing a connection to the grid.

There are an estimated 496,000 street lights in Massachusetts alone. These lights collectively use approximately 305 GWh/yr [10]. Assuming the cost of electricity is \$0.14/kWh running these lights alone cost Massachusetts over \$42,000,000 a year.

	Existing 70W HPS	LED 3-array	Optional LED2-array
Total power draw	97W	72W	48W
Average illuminance	3.54 fc	3.63 fc	2.42 fc
Maximum illuminance	7.55 fc	5.09 fc	3.40 fc
Minimum illuminance*	1.25 fc	1.90 fc	1.27 fc**
Max/Min Ratio (uniformity)	6.04:1	2.68:1	2.68:1
Energy consumption per luminaire***	425 kWh/yr	311 kWh/yr	210 kWh/yr
Energy savings per luminaire	--	114 kWh/yr (26.8%)	215 kWh/yr (50.6%)

Figure 4: Comparison of power efficiency between HPS and LED street lights [2]

Many of the street lights are older model high pressure sodium (HPS) and metal halide (MH) street lights which draw 97W each. In recent years these older models of street lights have been phased out in favor of more efficient LED street lights. A 3-array LED only draws 72W, while a 2-array light uses 48W [13]. Figure 4 above shows some other statistics regarding LED vs. HPS lights. Some LEDs use as little as 20W [1].

2.4 Generator

2.4.1 Alternator

The ability to use the mechanical energy of the ramp to power streetlights requires a conversion to electrical energy. The team decided that the simplest way to convert the rotational mechanical energy into electrical energy would be to use an alternator.

Alternators use mechanical energy to generate electrical energy in the form of an alternating current. They operate based on the principles of Faraday’s law which states that an electric field is created in a conductor when it experiences changing magnetic fields. Changing magnetic fields can be the result of a conductor moving through a magnetic field or magnetic fields moving around a stationary conductor. The electric field that is created causes current in

the conductor. This current can then be harnessed as electrical energy. Figure 5 shows how moving a coil of conductive material through a magnetic field causes current to flow.

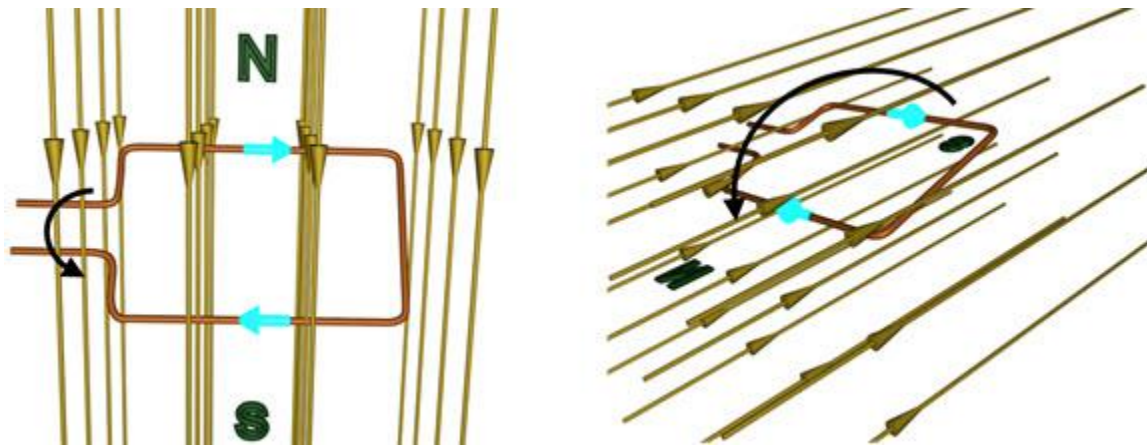


Figure 5: Current generated by an armature from two angles [20]

To create current using a conductor and a magnetic field, generators use a magnetic field and a conductive armature. One of these needs to remain stationary and is referred to as the stator of the generator. The other needs to move and is referred to as the rotor. There are many methods used to create the magnetic field. The simplest way to create a magnetic field is to use permanent magnets. Permanent magnets create their own magnetic field, so they can be used to generate the field for the generator.

Generators that use permanent magnets for their magnetic field are called permanent magnet generators (PMG), permanent magnet alternators (PMA), or magnetos. Figure 6 shows a PMG which uses magnets to generate a magnetic field in the rotor and a winding of conductive material to act as the static armature.

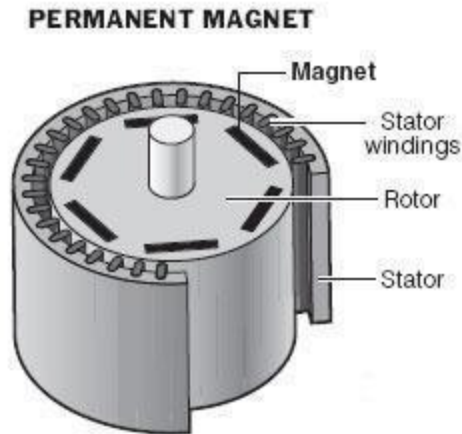


Figure 6: Diagram of a PMG [12]

Rotating the magnet causes the direction of the current to repeatedly alternate which causes the output electrical energy to be in alternating current (AC). The frequency of the output is governed by the equation $f = \frac{PN}{120}$, where P is the number of poles in the rotor and N is the rotor speed in RPM.

2.5 Speed bumps

Speed bumps and speed humps (shown below in Figure 7) are two different in-road obstructions that are used to check the speed of passing drivers. Speed bumps tend to be a more jarring experience because they are a tall, but relatively narrow raised section of pavement. Speed bumps tend to be “between three and six inches [tall and] only one to three feet long” [6]. The dangers of speed bumps are due to the fact that because of their design, they can be uncomfortable for drivers and cause damage to a vehicle’s suspension. Also, if taken at high speeds, a speed bump can lead to a driver losing control of their vehicle. Speed humps, on the other hand, are gently raised sections of asphalt that extend over the entire roadway surface. Speed humps are at a max of “three to four inches [tall]... and a max length [of] 12 feet” [6]. Speed humps are designed to “create a gentle rocking motion at low speeds,” but are still capable of causing a jolt to the vehicle at higher speeds which alerts the user that they are going too fast [6]. A speed hump is designed to reduce a vehicle’s speed to around 15 miles per hour [6].



Figure 7: Speed bump vs. speed hump [6]

This all amounts to the G-forces experienced by the passengers operating the vehicle. It is key to a successful system to not impede on the drivers roadway experience. In a study where the average G-forces were measured from GPS systems on the vehicles, drivers were asked to accelerate and then brake as quickly as they felt comfortable. The study found that drivers do not feel comfortable with negative accelerations greater than 1.6m/s^2 [21]. So, our device will avoid making drivers decelerate faster than 1.6m/s^2 to prevent this discomfort.

Our project looks to take advantage of the fact that all of these vehicles decelerate every day on off ramps and with the mechanisms we have researched we decided we wanted to create a better green device that is simple and effective at harvesting wasted kinetic energy of vehicles exiting highways. The next chapter discusses some initial concepts and ideas to create such a system.

Chapter 3. Design model

There were a few initial models created to have a system that will both decelerate cars and generate power. We first began by brainstorming a number of simple solutions to the problem of slowing vehicles down on off-ramps. For this played around with the idea of using painted lines on the road surface that got wider apart which is a visual cue to the driver and makes them unconsciously slow down. We also played around with the idea of doing some sort of a grated surface which would cue the driver they were on an off-ramp and cause them to reduce their speed. In changing the road surface, we also thought about creating a “sticky” surface which would have a higher coefficient of friction than asphalt or concrete and cause the car to slow down naturally without effort from the brakes. These ideas, had an obvious flaw of they only addressed the portion of the project which was assisting drivers in slowing down. Also, even though the idea of lines is simple and cost efficient, the other two ideas would cause increased wear on the tires and would become ineffective once the surface wore down.

From here we then brainstormed other ideas for generating electricity from a car driving on an off-ramp. Cars, with frames being made primarily out of ferrous steel, are inherently magnetic. If we were able to mount magnets to cars on a road, then we would be able to harvest the energy by imposing a change in flux in coils imbedded in the road surface which would create a voltage, therefore creating energy. However, this system would be impractical because we would have to put strong magnets on all of the cars on the road.

The next idea was a simple ramp and springboard concept. This simple concept transferred the car's kinetic energy into potential by going up an incline and then driving onto a springboard that can harvest the downward linear motion as pictured below in Figure 8.

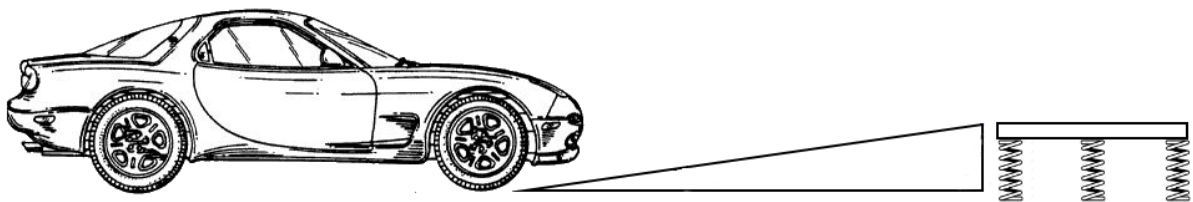


Figure 8: Springboard design

This design was not selected since it only harvests the vehicle's downward force. Much more of the car's energy is in the direction it is traveling so it was decided that a better design could harvest both directions of energy to be more efficient. This led us to the design we selected, a ramp but one which is hinged at the beginning so that a vehicle's forward momentum and its weight combined work to depress the ramp. The next consideration for the design of this ramp was how to go about converting linear downward motion to rotational motion for power generation. Initially the design was to use a rack and pinion to drive the generator like pictured below in Figure 9.

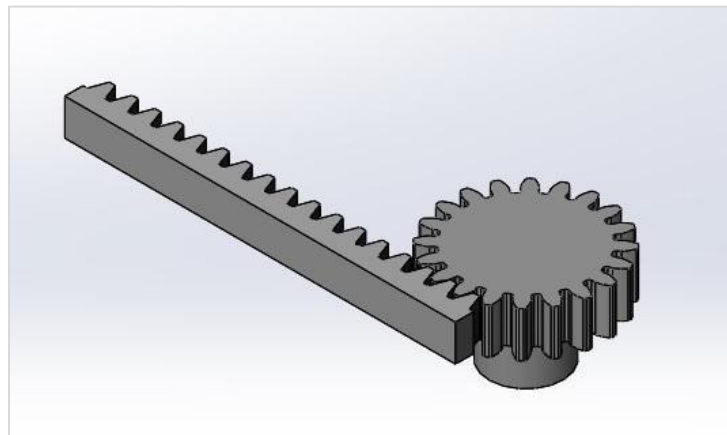


Figure 9: Rack and pinion

Here the rack would have the linear motion of the ramp depressing to spin the pinion and rotate a generator. However, it was decided to instead use a slider crank since parts were less complex and easier to produce and they both have the same end result of converting linear motion to radial motion. Creating a pivoting ramp does still require a method of returning the system to its initial position after actuation so we decided springs at the end of the ramp was the best way to achieve this.

Since the system we are creating aims to aid the deceleration of vehicles on an off-ramp it lessens the wear on a vehicle's brakes while harvesting the waste energy because a stopping vehicle converts its kinetic energy to heat energy through friction losses in the brakes. In order to create estimates for the power generation of our system we modeled and described the behavior of a vehicle as it traveled over our system. From these models we were able to derive our original mathematical model for movement through our system.

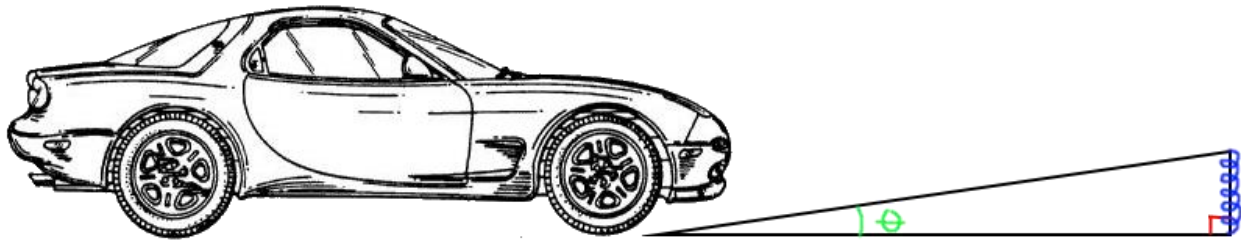


Figure 10: Before the ramp

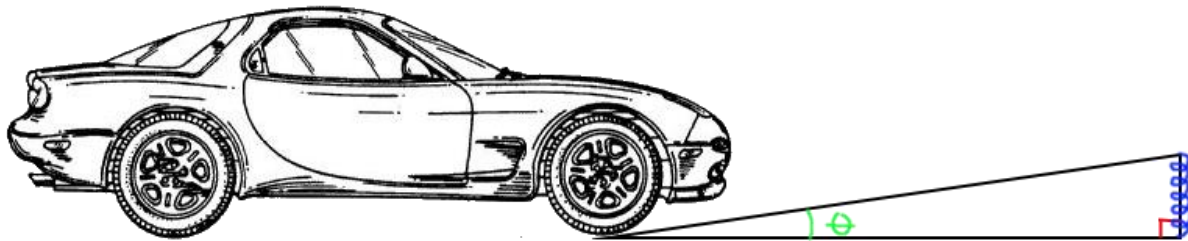


Figure 11: Beginning of ramp

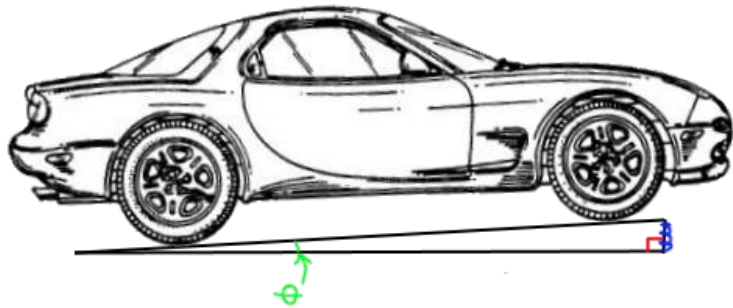


Figure 12: Just before the end of the ramp

The three images shown above give an idea into how our system operates. Figure 10 shows the vehicle approaching. Figure 11 is the moment a vehicle makes contact with the ramp and Figure 12 is when a vehicle has almost reached the end of the ramp. A vehicle will approach at a given velocity and mass and begin to travel up the ramp. The portion of the ramp with the spring, along with the coefficient of friction of the ramp itself, are the mechanisms our system uses to absorb energy from the car. By absorbing this energy, our mechanism is slowing the vehicle down.

When we first began to develop a model we delved into the physics of traveling up a static ramp to determine a baseline for equations and graphs that we could reference when we began to model our dynamic ramp.

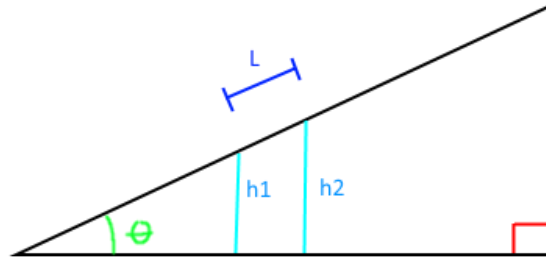


Figure 13: Static ramp design

By applying the conservation of energy equation to Figure 13 we were able to derive an equation which gave us the final velocity of a car at the top of the ramp. The conservation of energy equation states that the total initial kinetic and potential energy (KE and PE) will be equal to the final KE and PE of a system minus losses due to friction. In the equations in Figure 14 below, we used m to equal mass, v to equal velocity, g to equal the acceleration due to gravity, h to equal the height, μ to equal the coefficient of friction of the tire on asphalt, and N to equal the normal force of the car driving up the ramp.

$$KE_1 + PE_1 = KE_2 + PE_2 - \text{Losses (Friction)}$$

$$(1/2)mv_1^2 + mgh_1 = (1/2)mv_2^2 + mgh_2 - \mu NL$$

$$L = (h_2 - h_1) / \sin(\theta) ; N = mg \cos(\theta)$$

$$(1/2)mv_1^2 + mgh_1 = (1/2)mv_2^2 + mgh_2 - \mu mg \cos(\theta) [(h_2 - h_1) / \sin(\theta)]$$

$$(1/2)mv_1^2 + mgh_1 = (1/2)mv_2^2 + mgh_2 - [\mu mg(h_2 - h_1)] / \tan(\theta)$$

Mass cancels from each term:

$$(1/2)v_1^2 + gh_1 = (1/2)v_2^2 + gh_2 - [\mu g(h_2 - h_1)] / \tan(\theta)$$

Solving for v_2 :

$$A : v_2 = \sqrt{v_1^2 - 2g(h_2 - h_1) + [2g\mu(h_2 - h_1)] / \tan(\theta)}$$

Figure 14: Conservation of energy equation

With the equation “A” we came up with we were able to calculate the final velocity when given the initial velocity and the distance traveled along the ramp L (shown in Figure 13 above). If we took L to be infinitely small and used software to iteratively solve for final velocity we could develop graphs of position vs time and acceleration vs time of the static ramp as see below in Figure 15.

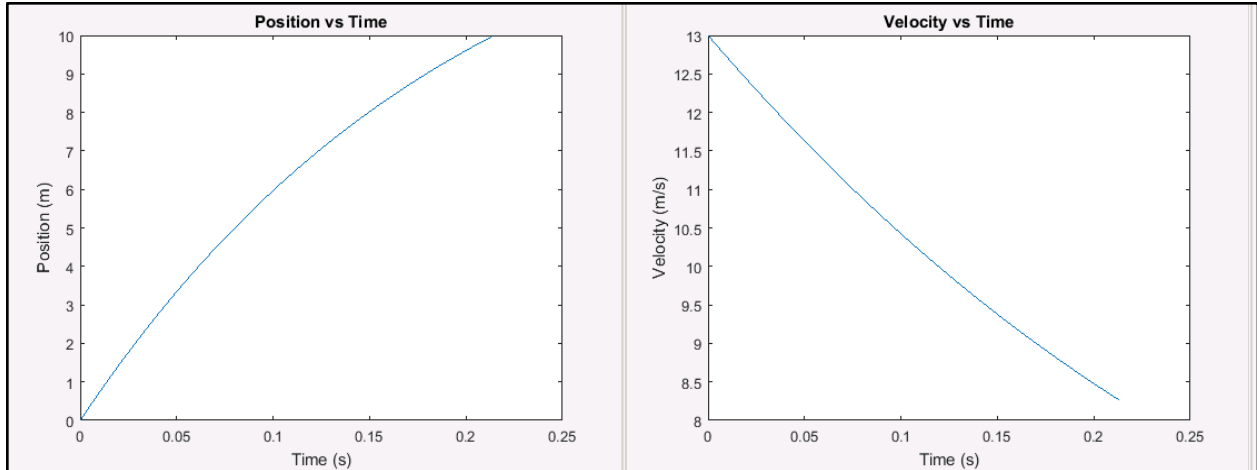


Figure 15: Behavior alongside a static ramp

Once we had the graphs performing the way we thought they should, we had the basic way to express the behavior of a car on a static ramp we were able to further refine the model to be more accurate. Figure 16 below describes what our actual device will look like. From this figure we were able to create a few more expressions to describe the system.

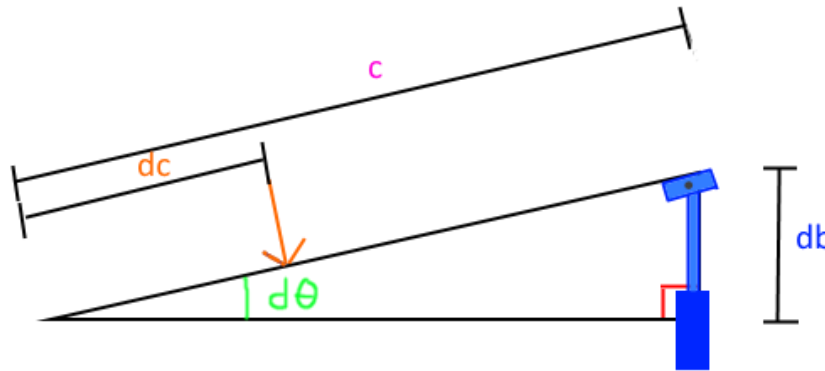


Figure 16: Ramp with a spring on the end

In order to calculate the spring force, we took the ramp and made it a cantilever beam. On that, shown in Figure 17 below, we drew a free body diagram (FBD) which showed all of the forces acting on this portion of our system.



Figure 17: FBD of ramp treated a cantilever beam

In Figure 17 we defined c to be the total length of the ramp, dc to be the instantaneous position along the ramp relative to the origin, $d\theta$ to be the instantaneous angle, db to be the instantaneous height of the ramp, and the upward force at end of the ramp to be the reaction force due to the spring. The force on the spring has two components to it due to the constantly changing angle of the ramp. However, for our system we chose a small initial angle in order to make the assumption that the ramp can be treated as quasi static.

$$\cos(\theta) \approx 1 - \theta^2 \text{ [rad]}$$

$$\cos(10) \approx 1 - 0.174533^2 = 0.97$$

$$\cos(0) \approx 1 - 0^2 = 1$$

Figure 18: Theta approximation justification

We were able to make this assumption of a quasi-static ramp as long our θ is below 10° (0.174533 rad). Based on Figure 18 above we approximated that the cosine of θ is always between 0.97 and 1, which averages out to 0.985. This means for any θ in between 10° and 0° the maximum error will be 1.5%. Since we made this assumption the reaction spring force is as shown below in Figure 19.

$$F = k(d-db)\cos(d\theta)$$

$$F = k(d-db)0.985$$

Figure 19: New reaction at the spring

Using the FBD of the ramp in Figure 17, we took moments about the base which gave us an equation relating instantaneous position and instantaneous height at the end of the ramp as shown in Figure 20 below.

$$\Sigma M_{\text{base}} = -mgdc + 0.985k(b-db)c = 0$$

$$mgdc/(0.985kc) = b-db$$

$$\mathbf{B} : db = b - mgdc/(0.985kc)$$

Figure 20: Equation B, solving for db

We solved the equation “B” (Figure 20) for db. We used the geometry for a right triangle which relates dθ and dc to db to substitute in equation “B” for db to solve for dθ (Figure 21).

$$\sin(d\theta) = db/c$$

$$\sin(d\theta) = (b - mgdc/[0.985kc])/c$$

$$d\theta = \sin^{-1}\{(b - mgdc/[0.985kc])/c\}$$

Figure 21: Equation solved in terms of dθ

The equation for dθ in Figure 21 can be expressed by the graph in Figure 22 which shows the curve of how dθ changes with respect to its instantaneous position.

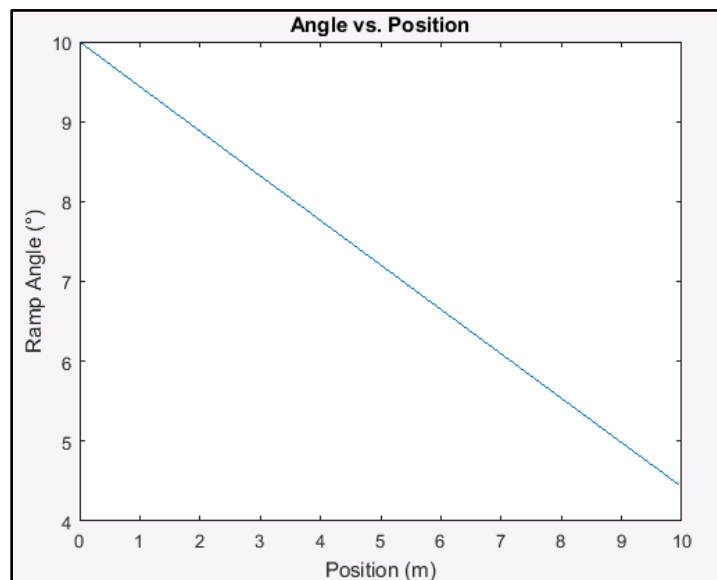


Figure 22: Instantaneous angle vs. instantaneous position

We also performed a translation to instantaneous position to solve for time by using the equation:

$$V_0t + (1/2)at^2 - dc = 0$$

In this equation, acceleration (a) is the component of gravity in the direction of motion of the car, which can be described as deceleration due to gravity. After making this translation we are able to plot the following graphs shown in Figure 23.

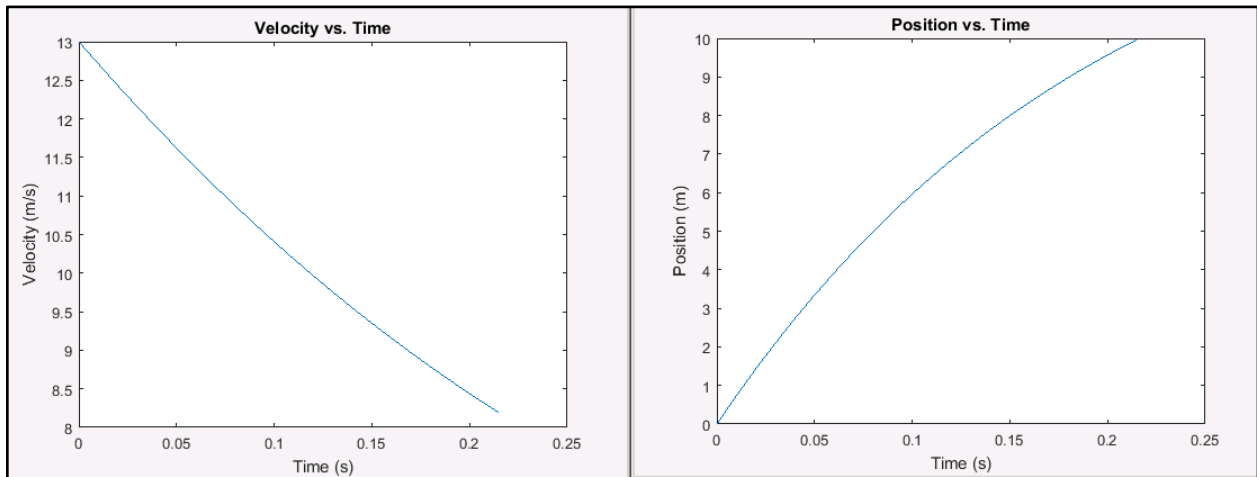
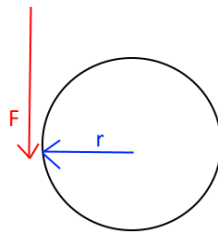


Figure 23: Behavior along a dynamic ramp

Once we developed some governing equations of motion we began to calculate the potential output of the system.



$$T = Fr$$

Figure 24: Torque

Given the equation for torque is as shown above in Figure 24 we calculated the downward force of the system as follows:

$\Sigma F_{\text{downward}} = \text{Weight of car} - \text{Force absorbed by the spring}$

$$\Sigma F_{\text{downward}} = mg - kb$$

Designing the diameter of the wheel being torqued to be equal to the stroke of the system will result in one half of a revolution. This would lead the wheel to be designed with a diameter equal to the distance the ramp compresses **b**:

$$T = (mg - kb)b$$

Manipulating another equation for torque in Figure 25 below can aid in solving for the speed at which our system produces this torque. In this equation **I** is inertia of the output shaft and **α** is the angular acceleration.

$$T = I\alpha$$

$$I = 0.5mr^2$$

$$m = \rho V = \rho (\pi r^2)h$$

$$I = 0.5 \rho (\pi r^2)h r^2$$

$$I = 0.5 \rho (\pi b^4)h$$

Figure 25: Derivation for inertia

In this derivation the first line is the inertia for a solid cylinder as in the case for the system, the output shaft. After substituting mass in terms of volume and density we end up with an equation for inertia of the output shaft that depends on the radius we choose, in this case $r=b$. Substituting this back into the other torque equation gives as follows:

$$(mg - kb)b = [0.5 \rho (\pi b^4)h]\alpha$$

$$\alpha = (mg - kb)b / [0.5 \rho (\pi b^4)h]$$

Now there is an equation for the torque and angular acceleration of the output shaft. Since angular acceleration is angular velocity per unit time and time was previously modeled in MATLAB (see Appendix B for code), angular velocity can be solved for shown in Figure 26 below.

$$\omega/t = \alpha$$

$$\omega = \alpha t$$

$$\omega = t(mg - kb)b / [0.5 \rho (\pi b^4)h]$$

$$\omega = t(mg - kb) / [0.5 \rho (\pi b^3)h]$$

Figure 26: Angular velocity equation

The unit for ω is rad/s which can be converted with a factor of 60 seconds over 2π to result in rotations per minute. With the models and equations developed the system's mechanical output torque and speed can be calculated with the following equation:

$$P = T\omega$$

Chapter 4. Methodology

Our group moved on to creating a working model and building the individual parts that were combined into our prototype.

4.1 Coil Design

Once we decided on the generator, we needed to design the coils that would be used in the generator. The design of the coils followed an iterative process, where a single coil was made, tested, and improved in the next version.

4.1.1 Coil dimensions

The next objective was to determine the optimal dimensions of the coils that we would use with the generator. The team decided to use multilayer coils because they would be easiest to construct. Multilayer coils consist of winding an insulated wire around an open air gap.

When constructing a multilayer coil, it is important to consider a few parameters. The primary considerations are the number of windings on the coils and the size of the central air gap. The more windings in a coil, the greater the output voltage of the system, as shown in Faraday's law in Figure 27 below [15].

$$L = -N * \frac{\Delta BA}{\Delta t}$$

Figure 27: Faraday's law for voltage induced in a coil

In this equation, N is the number of windings in a coil, and it is directly proportional to the output voltage of the system. It was important to choose enough windings to induce enough voltage without making the coils too large or using too much wire. The second major consideration is the size of the air gap. The air gap in the center needs to be large enough to capture the magnetic flux from the generator's magnets, but small enough to remain space-efficient. To get the proper size, the air gap needs to be slightly larger than the magnets in the generator. This was easy to determine once the team found the magnets that we would use on the generator.

A third consideration when creating a multilayer coil are its dimensions. The coil will always consist of a cylindrical air gap with wire wound around it. However, the coil could be

wound in different dimensions. These dimensions are the height of the coil (c below), the depth of the coil (b below), and the radius of the coil (a below). A diagram showing these dimensions is shown in Figure 28 below.

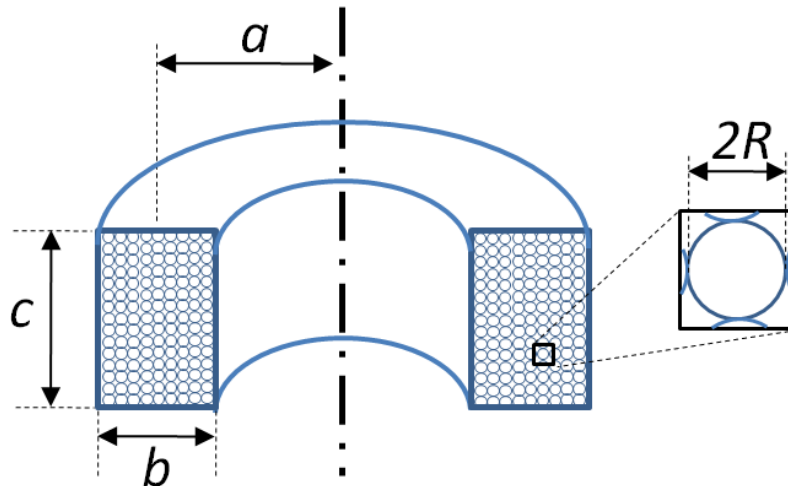


Figure 28: Dimensions of a multilayer coil [20]

These dimensions need to be chosen to maximize the inductance of the coil. Greater inductance leads to greater flux through the coil, increasing the induced voltage. The optimum dimensions for a coil that create the highest inductance for a given length of wire was discovered by Morgan Brooks. Brooks found that the maximum inductance is created when the ratio of $a:b:c$ is 1.5:1:1 [4]. This means that the coils the team produced would need to be close to these dimensions, with an equal length and depth and a radius of 1.5 times the length or depth [7].

To summarize, we needed to construct coils that would have enough turns to produce the correct voltage, an air gap that was larger than the magnets that our generator used, and dimensions such that the ratio of $a:b:c$ is 1.5:1:1.

We decided that 3D printing spools to wind the coils onto would be the most efficient and aesthetically pleasing way to make the generator coils. The plastic involved in 3D printing is PLA which is not conductive, so it will not influence the performance of the coils. Having a solid base to wind the coils around would also make production more efficient and simplify coil mounting.

The voltage output of the coils was tested with a “pendulum test”. This test consisted of swinging a 0.125” steel pendulum with a magnet attached in front of our coil and measuring the output voltage. This allowed us to control the speed of the magnet to some degree and test the coil a range of low speeds. The speed was measured by measuring the distance that a magnet

passed by our coil and comparing it to the speed of the resulting waveform on the oscilloscope. The speed was converted to an RPM for a 6” diameter wheel with the following equation (Figure 29).

$$RPM = 60 * \frac{u}{C}$$

Figure 29: RPM equation

Where “u” is the velocity of the magnets in m/s and “C” is the circumference of a 6” diameter wheel in meters. With this, the pendulum test estimated the peak voltage that a given coil would produce under a range of RPM values.

The first spool (Figure 30) had flanges that were 0.125” thick. The spool was 0.75” tall, so the coil would have length $c = 0.5$ ”. The inner diameter of the coil was 1.25”, which was enough to accommodate our 1” diameter magnets. We started with 100 turns around the spool, wound by hand. After winding, the depth “b” of the coil was 0.25”. The results of the tests can be seen in Appendix C. The first coils gave a maximum value of 0.536 peak voltage at 93 RPM.



Figure 30: First generation coil

The first coil illuminated many places for improvement. The flange thickness could be reduced, allowing the magnets to get closer to the coil. The a:b:c dimensions were 0.75:0.25:0.5, a ratio of 3:1:2, but a brooks coil has a ratio of 3:2:2 [4]. The coil had a low voltage, which could be improved by adding more turns. Finally, the group realized that adding a hole for a steel core

to the center of the coil would improve the flux through the coil and the efficiency of the generator. With these improvements in mind, a second spool was designed.

The second spool (Figure 31) had flanges that were 1/16" thick. The spool was 0.625" tall, giving length $c = 0.5$ ". The inner diameter was left at 1.25" to fit the magnets. A hole was left in the center of the spool with radius 0.75". To improve the voltage, this spool was wound for 200 turns. This also increased the depth to $b = 0.4$ " and the radius to $a = 0.825$ ". The ratios for this coil were 2.06:1:1.25. Although the "a" value is a little large, the ratios are close the brooks coil values of 1.5:1:1. The peak voltage of the new coil were improved, with a maximum of 1.42v peak at 104 RPM.

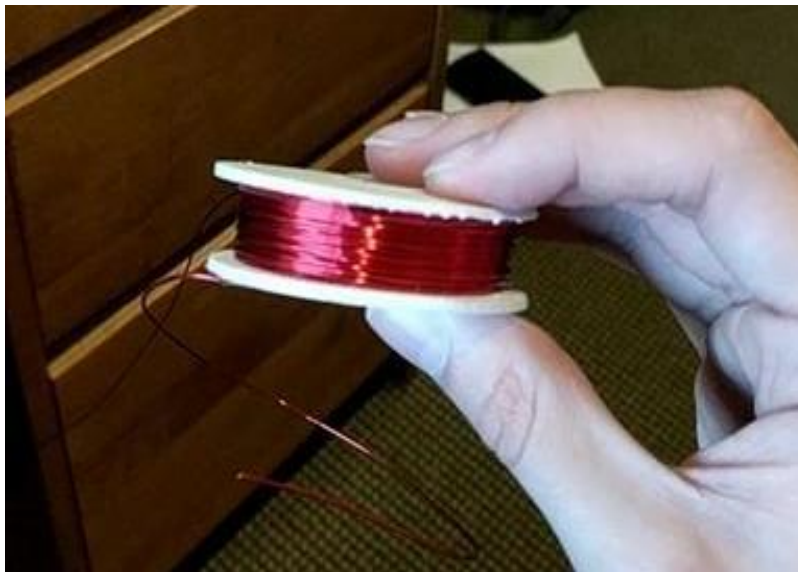


Figure 31: Second generation coil

Overall, the voltages were about twice as large as the previous values, which was expected because the turns in this coil was doubled. This coil was better, but still had room for improvement. The hole for the steel core could be expanded to 1" without risking the strength of the spool, and a larger core would improve the flux. At this stage in production, we also found that slightly reducing the outer diameter of the spool flanges would allow us to fit 4 coils on either side of the magnet wheel. So next iteration featured a coil with a larger core hole and a lower flange diameter to accommodate 4 coils.

The final coil design featured spools with a 2.1 inch flange diameter. The spools are 0.625" tall and feature a 1" diameter center hole for the steel cores. Each coil has 200 turns of wire around the inside with a starting diameter of 1.25". The final spools have dimensions that

are close to a brooks coil and a large center hole for a steel core. The spools also have flanges that are large enough to cover the wire and small enough to fit 4 coils on a 6” diameter steel wheel. Half of the coils were fit with 1” diameter steel rounds, and the other half were left without. Testing was later performed on both sets of coils to determine if the prototype would be finished with or without steel cores in the spools.

4.2 Intersection area

When analyzing the results of our coils, it was important to know all of the parameters of them. The relevant parameters when solving for voltage are defined by Faraday’s law. “N” the number of turns, was known because we made the coils ourselves. “B” the magnetic flux density, is difficult to estimate and is easiest to find by solving backwards when the other parameters are found. The last parameter is the change in area related to the intersection between the air gap of the coil and the area of the magnet, dA/dt . This area could be found by solving for the intersection between 2 circles over time. To solve this, we created a “C” function that calculates the area intersected between 2 circles over a given time, giving the derivative dA/dt . The code for the function can be seen in Appendix D. The calculation that the code performs is shown in Figure 32 below.

$$\begin{aligned} \text{area} &= \text{area}_{s,1} + \text{area}_{s,2} - \text{area}_{t,1} - \text{area}_{t,2} \\ &= A_r^2 \sin^{-1}\left(\frac{y}{A_r}\right) + B_r^2 \sin^{-1}\left(\frac{y}{B_r}\right) - y\left(x + \sqrt{B_r^2 - A_r^2 + x^2}\right) \end{aligned}$$

Figure 32: Formula for intersection between two circles

In this equation, $\text{area}_{s,1}$ and $\text{area}_{s,2}$ are the areas of the arcs seen in the next figure. The arcs in Figure 33 are the arcs of each circle that span the intersection points between the two circles. If the two arcs are summed, and the area of their triangular portions, $\text{area}_{t,1}$ and $\text{area}_{t,2}$, are removed, only the area of the intersection remains [10].

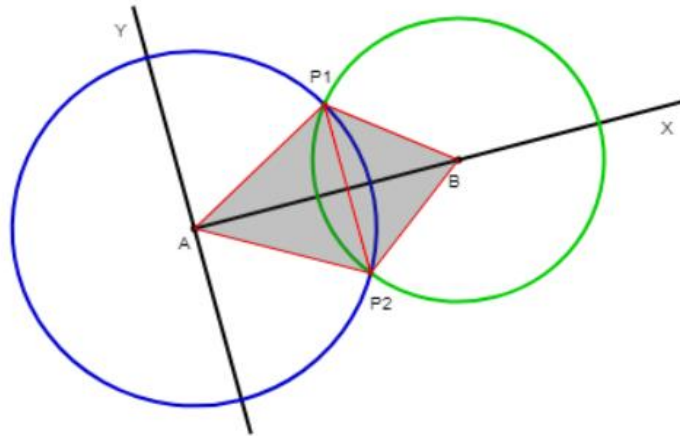


Figure 33: Intersecting circles' connecting area

In the formula, A_r and B_r refer to the radius of the circles A (blue) and B (green). “y” refers to the y-coordinate of the intersection point (- y would give the y-coordinate of the lower intersection point). “x” refers to the x-coordinate location of the two intersection points (given that the origin is the center of circle A). The equations used to calculate x and y are shown in Figure 34 below.

$$d = \sqrt{(B_x - A_x)^2 + (B_y - A_y)^2}$$

$$x = \frac{A_r^2 - B_r^2 + d^2}{2d}$$

$$y = \sqrt{A_r^2 - x^2}$$

Figure 34: Formulas to calculate x and y

In the equations shown above, A_x and B_x are the x-coordinates of the center of circles A and B, and A_y and B_y are their y-coordinates. d is the distance between the centers of the two circles, calculated as an intermediate term to make the formula for x more readable. Once we had these formulae, we created the “c” function to run the numbers and calculate the area of intersection. Then move one circle, calculate the difference in area between the last intersection and the current one, and save the value of change in area/ change in time to get the derivative. The function saved these values to a .csv file named output.csv. With the output, we were able to enter the values into excel and compare them to our system. The C code is shown in Appendix

D. The code was run on a system that models our prototype system. The system had 2 circles of radius 1.25” and 1” and the 1” circle moved past the 1.25” circle at a speed corresponding to a 6” diameter wheel moving at 60 RPM. The resulting graph can be seen in Figure 35.

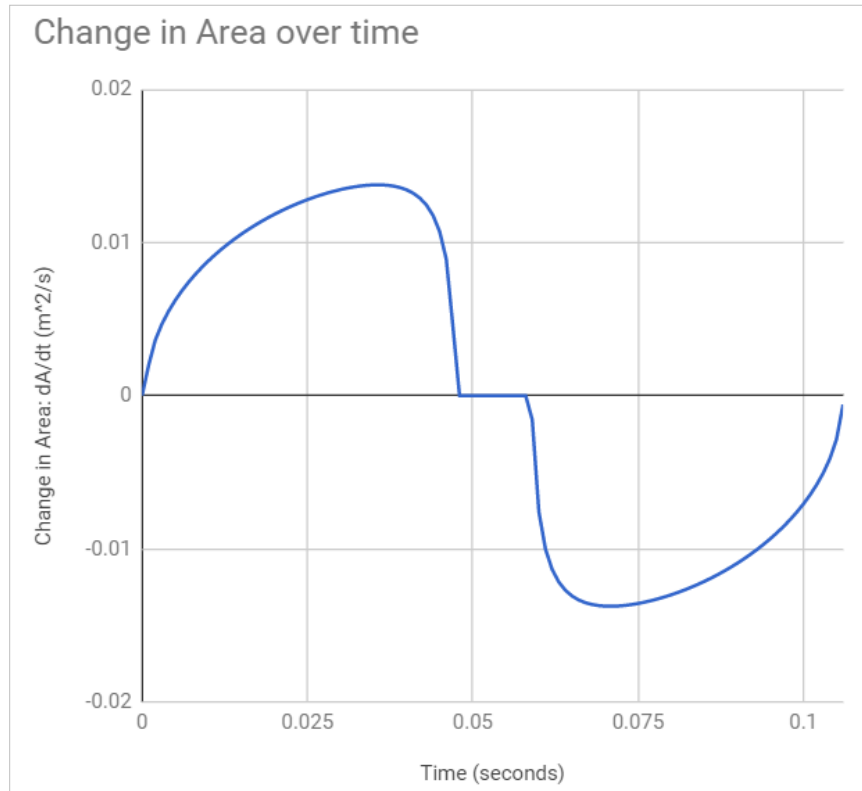


Figure 35: Results of code ran at 60 RPM

The maximum change experienced by the system was $0.013764 \text{ m}^2/\text{s}$. We compared the equation of Faraday’s law using $N = 200$ turns and $dA/dt = 0.013764$ to the peak output we measured on our coil at 60 RPM, $v = 0.96$ volts. Solving for B gave us a magnetic flux density of 0.349 T . Because our system is not fully efficient, we now knew that the magnetic flux density of our system was at least 0.3487 tesla.

4.3 Steel Saturation

With the design of the coils fleshed out, we had to consider the width of the steel wheel that held the magnets. The wheel did not have to be very wide to prevent warping. However, the steel had to be wide enough to prevent the magnets from saturating the steel. Saturation occurs when a metal can no longer contain the magnetic field generated by a magnet. In this condition, the path of the flux is weakened, and the magnets do not work at their maximum strength [17]. A

diagram showing saturated steel compared with non-saturated steel can be seen in Figure 36. With the saturated steel, the magnetic field lines pierce the steel, meaning that some of the magnet's strength is wasted on the wrong side of the steel. With the unsaturated example, all of the magnet field lines go through the steel and radiate out of the desired face of the steel.

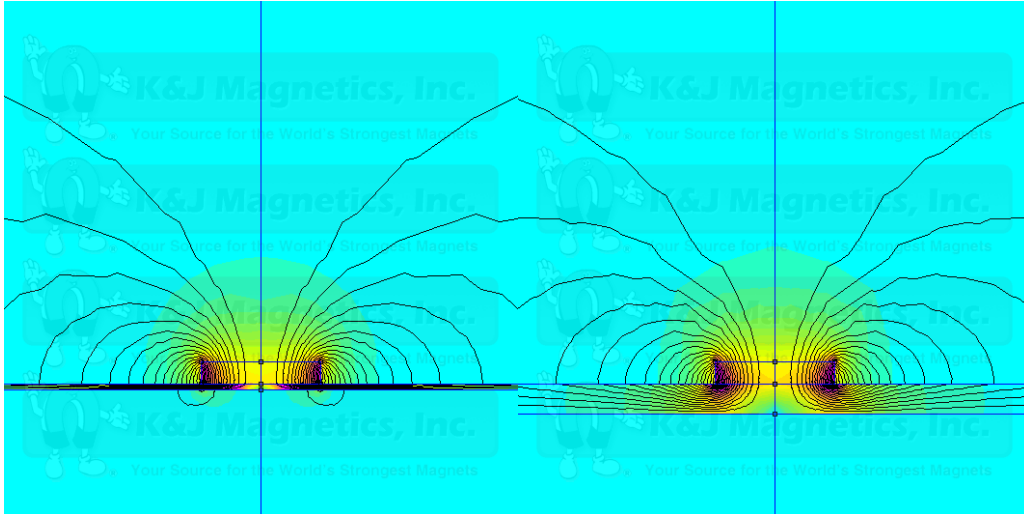


Figure 36: Saturated steel (left) vs. unsaturated steel (right)

To find the width of steel required to prevent saturation, an online calculator was consulted. Using the online calculator, the pull force of the steel was predicted to drop below 95% when the steel dropped to a thickness below 0.15" [17]. With this information, we knew that our steel wheel had to stay above 0.15" thick between the two magnets. With this information, we decided it would make the most sense to order a 0.5" thick round and mill down 0.0625" on either side to give the magnets places to sit. This milling would give us 0.375" between the two magnets, more than the 0.15" required.

4.4 Generator Design

To design the permanent magnet generator, our group considered the factors previously discussed. In addition, there are some additional design concerns for the entire system itself. First, we decided to have a generator with static coils and moving magnets. Setting up a generator in this configuration is much simpler because slip rings and brushes are required on generators with moving coils, but with static coils these factors can be mitigated.

With the decision to use static coils, the team designed a generator with a central steel wheel spun by the rotation of the crankshaft. This wheel would have magnets attached on each

side and coils suspended as close as possible next to the magnets. With this configuration, the compression of the ramp would rotate the wheel containing the magnets. This movement induces voltage in the coils, creating electrical power.

For a full-size version of the project, we would have a disk with 10 magnets on each side of the wheel and two stationary wheels with 6 coils each. For the prototype, we scaled this down to 5 magnets on each side of the wheel with 4 stationary coils on either side. A diagram of the final design is shown in Figure 37. Initially, the group decided on 3 coils on either side of the magnets, but while optimizing the coils we found that we would be able to fit 4 with slight modifications to the flange diameters.

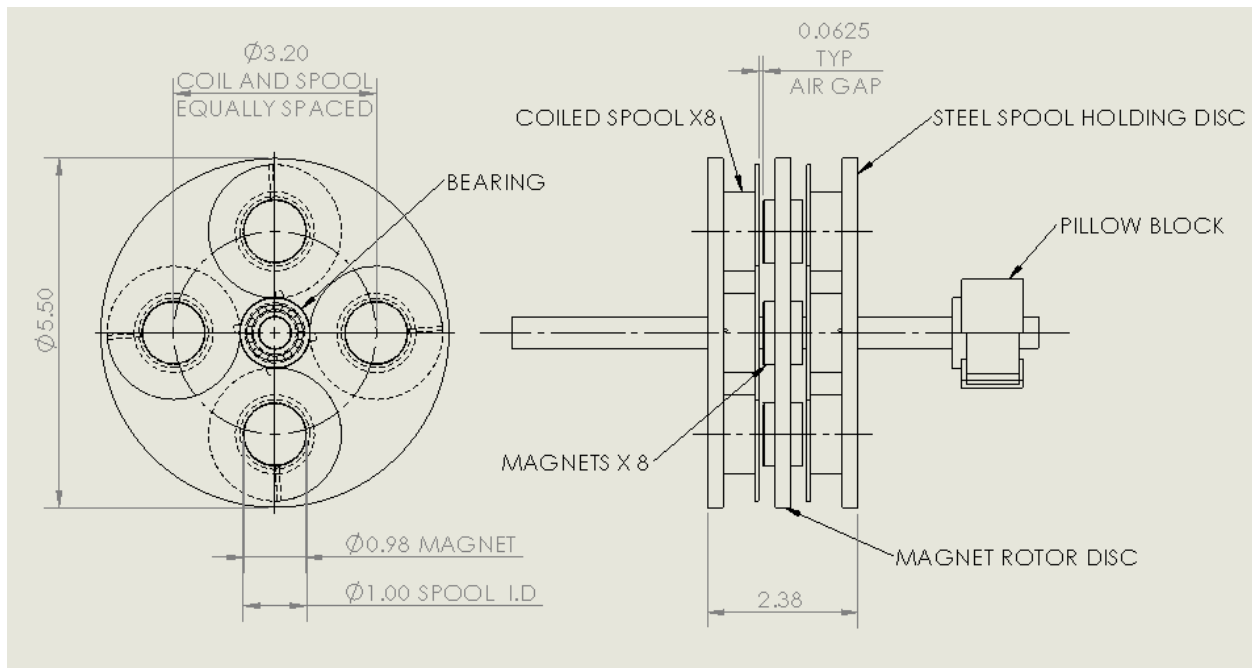


Figure 37: Diagram of generator design (measurements in inches)

4.5 Drill test

Once we finished the final set of coils, we tested the coils at higher RPM values. To test the higher RPMs, we used the steel wheels that holds the magnets and the coils. We attached the magnet wheel via press fit to the shaft that would turn it and attached the coil wheel with a bearing. This meant that the magnets would spin with the shaft while the coils could be held still. With the wheels in place, we put a single magnet on the magnet wheel and a single coil on the coil wheel. Afterwards, we attached a drill to the end of the shaft and used the drill to rotate the shaft at high speeds. The output voltage of the coil was measured with an oscilloscope. The

speed of the shaft could be solved for by measuring the time in between peaks of the oscilloscope output. The speed was recorded as the RPM of a 6'' diameter wheel at that speed. The results of the testing are in Appendix E: Single Coil Drill Test.

The first tests were done with a coil that contained a steel core. The test was repeated once with a different distance between the coil and magnet. The first test had a distance of 0.125''. During the test it became apparent that turning the coils this close to the magnet would be very difficult. A second test was performed with the coil and magnet 0.25'' apart. The group performed a third test on a coil without a steel core. The results can be seen below in Figure 38.

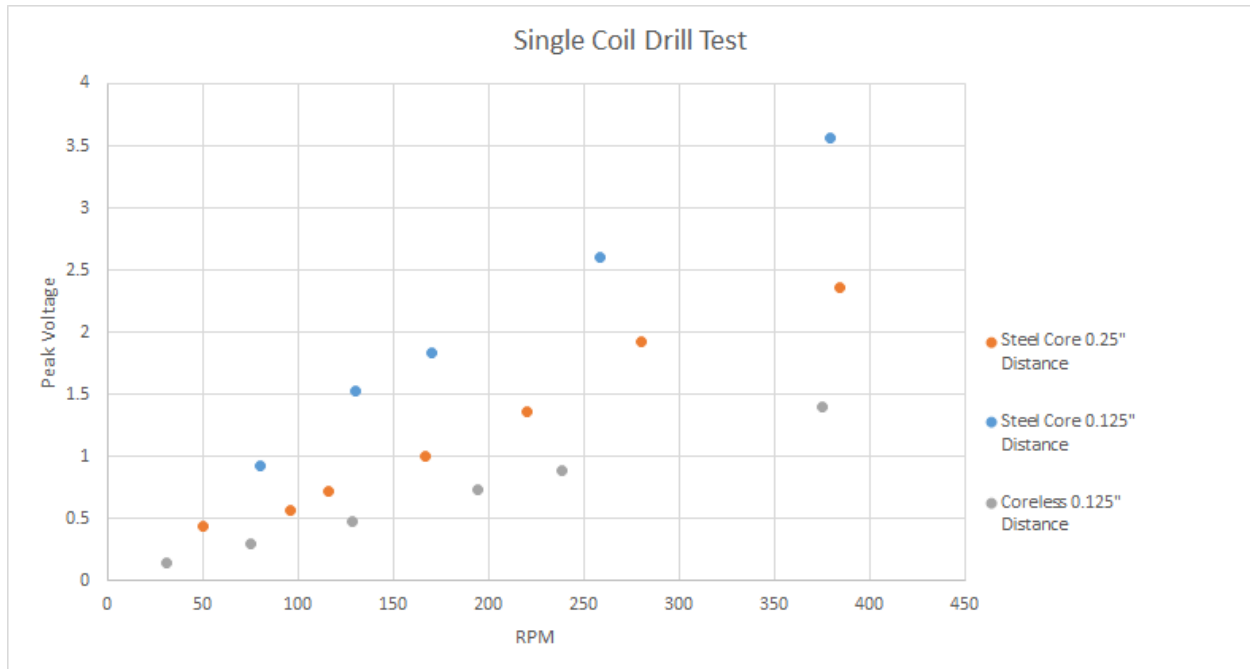


Figure 38: Coil test, core vs coreless

The coreless coil was much easier to spin, so we only tested it at a distance of 0.125'' because we were certain that the system would be able to spin 8 coreless coils.

The first test had a range of voltage values from 0.44 V at 50 RPM to 2.36 V at 384 RPM. The closest measurement to our expected 120 RPM value was 0.72 V at 116 RPM, so we would expect $8 * 0.72 = 5.76$ V from the coils at this distance with steel cores. The second test had a range from 0.92 V at 80 RPM to 3.56 V at 379 RPM. The closest to 120 RPM was 1.52 V at 130 RPM, leading to an expected output of 12.48 V. For the third test the range was 0.14 V at 31 RPM to 1.4 V at 375 RPM. The closest to 120 RPM was 0.472 V at 128 RPM, leading to an expected output of 3.776 volts. The data can be seen in Appendix E: Single Coil Drill Test. The best results were the tests with the steel cores, as expected. However, the group noticed that

during tests with the cores 0.125'' from the magnet, the magnet was moving on its wheel and the coil was getting ripped away from its wheel. In both tests with the steel cores, the system moved irregularly because torque became much greater when the core was directly across from the magnet. The group decided to design output circuits for the ideal steel case in case we resolved these issues as well as for the coreless case in case these issues could not be resolved. While the circuits were being designed, we also worked to test how much torque would be required to move each case and which would be more reasonable to use on our final design.

4.6 Output Circuit Design

With the expected values calculated, the group designed two output circuits for the system. Both circuits assumed the output voltage would be AC with a frequency of 8 Hz because the both cases assumed the system would rotate at 120 RPM and RPM determines frequency. The steel core circuit assumed a peak voltage of 12.16 volts, while the coreless circuit assumed peak voltage of 3.776 volts.

The steel core circuit included a full wave rectifier to convert the output to a lower DC voltage. Because the objective was to light LEDs, the lower voltage would still be high enough to light the LEDs, while the DC waveform would keep the LEDs lit constantly. The rectifier included a smoothing capacitor to keep the output more constant, keeping the LEDs lit. The output of the rectifier leads directly to some LEDs connected in parallel. This configuration allows the LEDs to share the lower voltage and be lit simultaneously. The circuit was tested in multisim and can be seen below in Figure 39. The voltage delivered to the LEDs is shown in Figure 40.

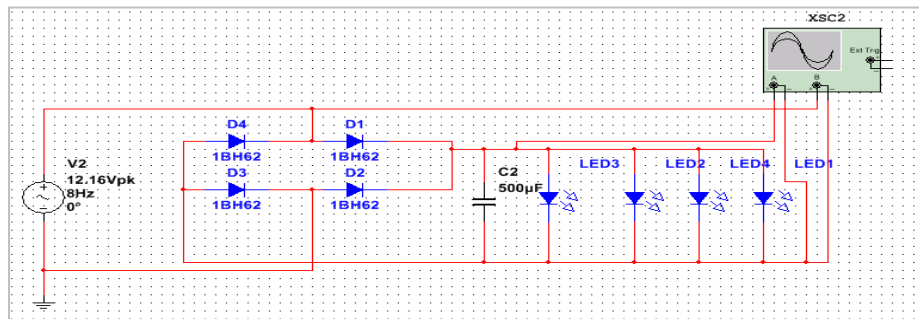


Figure 39: Multisim circuit

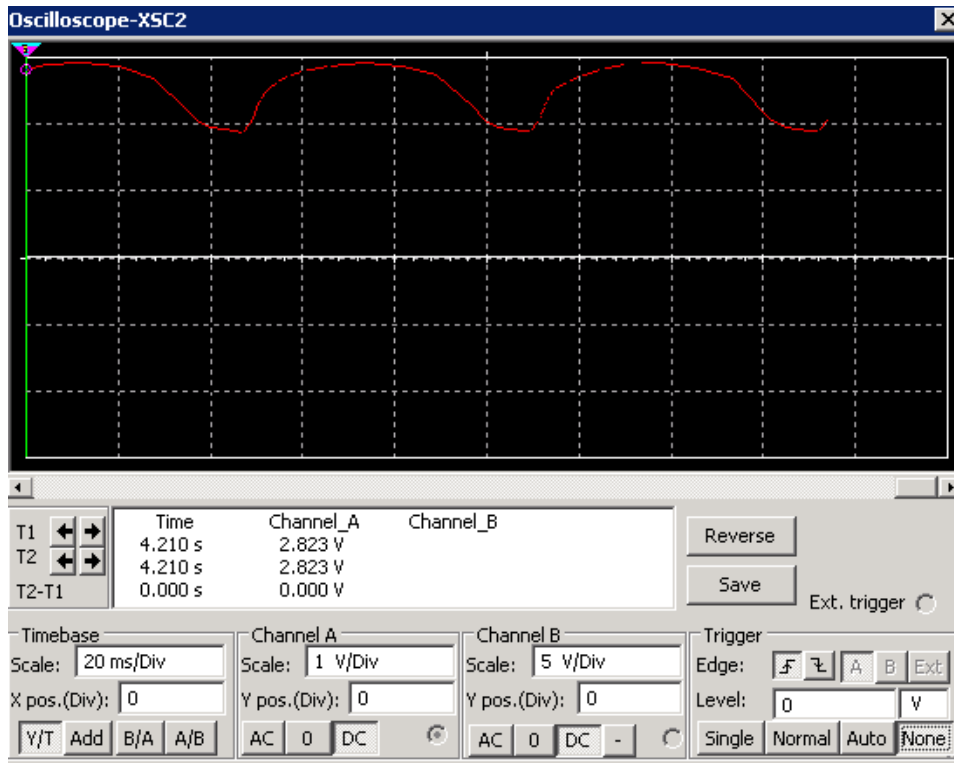


Figure 40: Multisim circuit LED voltage

The output changes slightly, with a peak of 2.9 V and a minimum value of 1.95 V. The minimum value is a little below the forward voltage drop of the LEDs of 2.1 V, so for a brief period the LEDs would dim when the system was moving. Outside of this period the LEDs would be brightly lit.

The coreless case was much simpler. Because the voltage was not high enough to support a full wave rectifier and still light LEDs, the LEDs were hooked directly to the output in parallel. Half of the LEDs ran from power to ground, while the other half ran backwards, from ground to power as seen below in Figure 41.

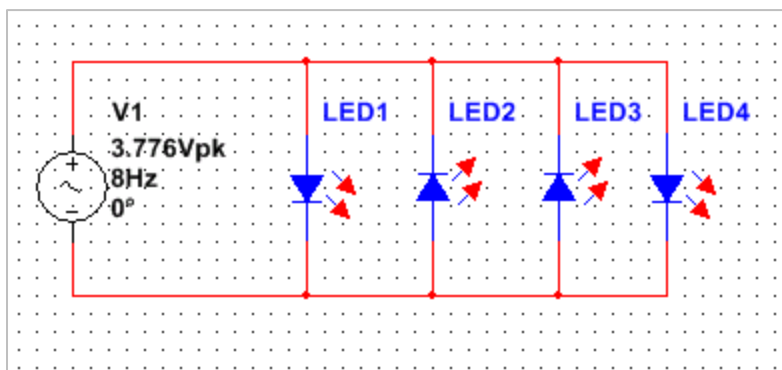


Figure 41: Schematic for prototype generator (coreless) output

The parallel alignment allowed many LEDs to share a voltage high enough to drive them. Because they only require 10 mA of current, having many LEDs in parallel did not draw much current from the system and the output could power them all. However, the AC output meant that only half of the LEDs would be lit at once, with the circuit alternating between those hooked up from power to ground and those hooked up from ground to power. Because this circuit was so simple it was not tested in multisim.

4.7 Machining

For our generator, we are using a steel rotating wheel that has magnets mounted on both sides which rotates within an additional two other steel wheels on either side that contain four spools of copper wire each. The wheel with the magnets on it is 0.375" thick with 0.0625" deep pockets for the magnets to sit in (Figure 42). The magnets are 1" in diameter, but when we measured them the diameter was actually 1.05" so the pockets are 1.10" in diameter to allow for removal of the magnets and to account for the slight variation in the size. The through hole in the center is 0.5" for the rod, which is press fit to the rod which rotates, conferring torque to the wheel.

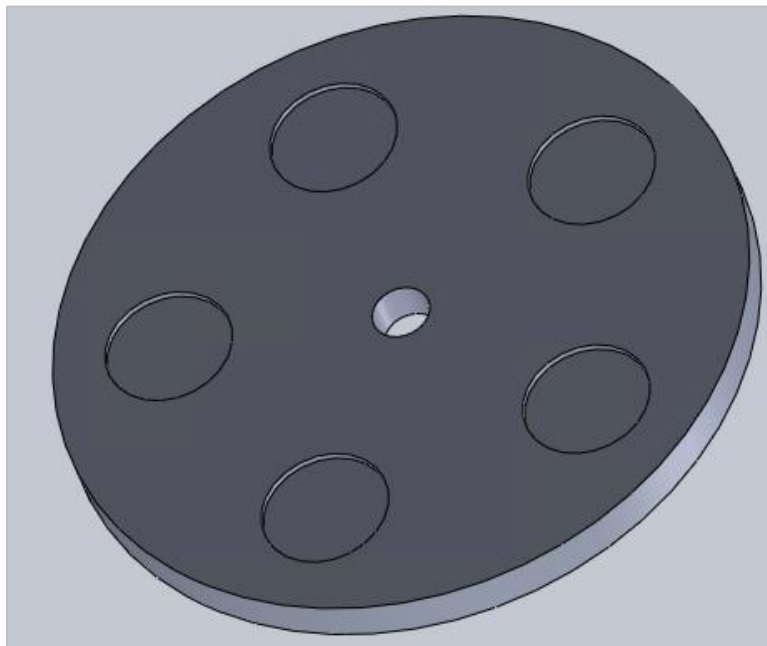


Figure 42: Generator wheel design

The raw steel we are using is 1045 high strength steel that starts out 6" in diameter and is 0.5" thick. To create the final part we needed, we had to machine down the part using a VM-2 Haas machine. To create the code for the computer numerically controlled (CNC) machine, we used Esprit to model the facing and pocketing operations that are required (Figure 43).

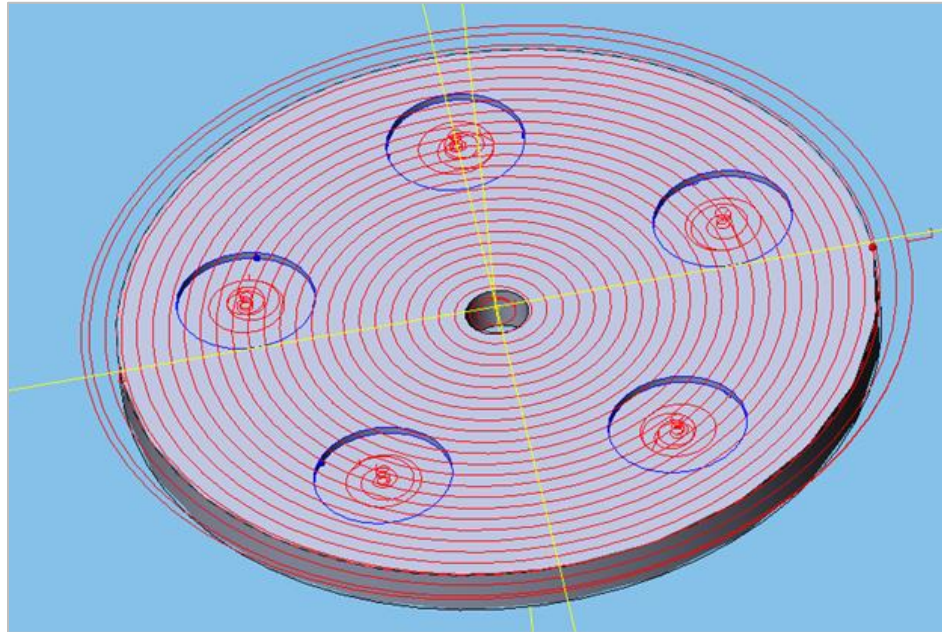


Figure 43: Esprit code for the generator wheel

This design, which is duplicated on both sides, uses a 0.5" ferrous end mill tool to do a facing operation that took off 0.0625" of steel from the top, creating a flat face for the rest of the pockets to be milled into the part. The next operation that is performed is the milling of the recessed pockets that the magnets sit into and the through hole, which both use the same tool as the facing operation. By taking 0.0625" off of each side of the part, the piece is milled down to 0.375" thickness. When the pocketing operation is complete, the steel between the magnets will be 0.25" thick, which is well above the 0.1 saturation limit.

As you can from Figure 42, our original plan was to maximize the number of magnets on the steel wheel by having 5 per side. However, as our team was mounting everything to create the finished generator we realized that this original plan was not going to work. With five magnets there would be a repeating pattern of n,s,n,s,n which would lead to two magnets being the same polarity adjacent to each other which would cancel out the voltage they would each generate. So, we modified our design to only use 4 magnets and put them at 90 degrees from each other at the same radius as the coils so they passed directly through the center of the coils.

For the stationary wheels, we used the same 1045 high strength steel stock to create a 0.5” thick wheel that has four pockets. The operations are similar (Figure 44), using the 0.5” ferrous end mill, we create the pockets for this new part.

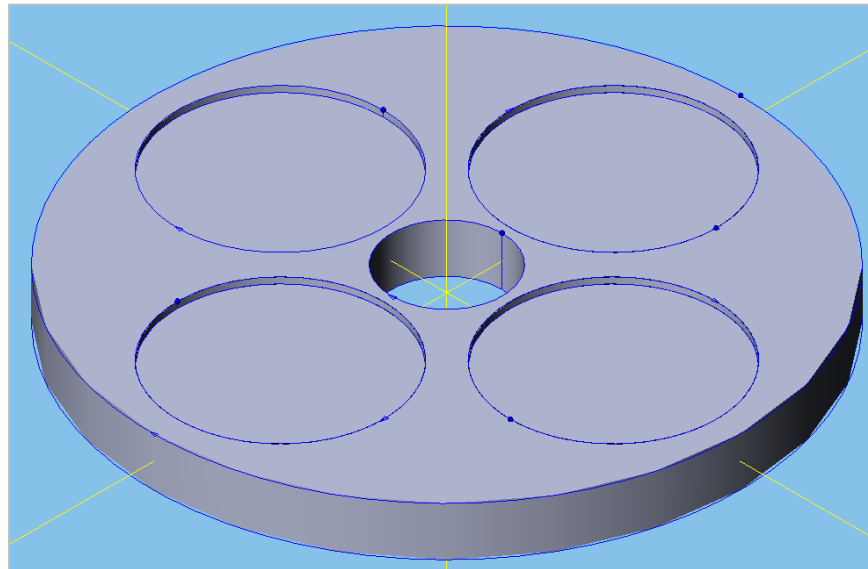


Figure 44: Esprit file for stationary generator wheel

The wheel has only four pockets, which are 2.1” in diameter, to allow for super glue and slight variation in the 2” diameter 3D printed part (Figure 44). The facing operation for the part will be taking off 0.03125”, which is enough to create a smooth, finished surface, but not too much to change the overall size of the part.

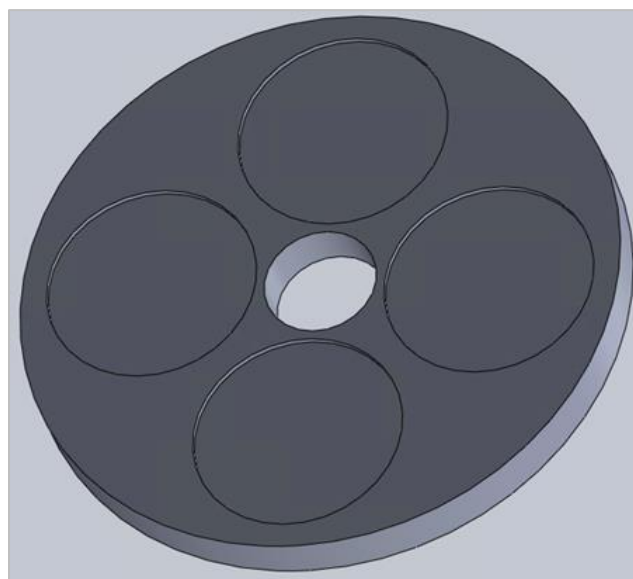


Figure 45: Stationary generator wheel

The pockets are 0.0625” deep, which is the depth of the flange on the coil. The coils will then be set into these pockets. The through hole in the center is larger than the rotating generator wheel to press fit a 1” bearing, which will allow for the rod to rotate freely.

4.8 Inertia calculations

The concept of this ramp is to be placed onto highway off ramps is that some of the kinetic energy which is lost to heat by the brakes is recollected. Since this is the case the ramp will be as wide as the off-ramp lane itself as seen in the following image (Figure 46).

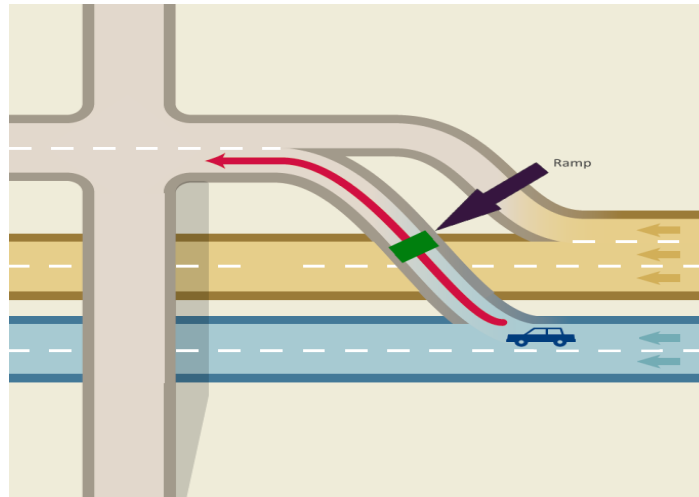


Figure 46: Ramp location

One of the main constraints behind designing a ramp like this is the high variance in vehicle weights. From our research we found cars could weigh anywhere from four hundred pounds to eighty thousand pounds. Because of this high vehicle weight variance the ramp must be able to handle the extremely high torques created by semi-trucks but also be gentle enough to allow for a motorcyclist to pass with no discomfort.

The first thing considered in the ramp design were the springs that hold the ramp up. Using Solidworks to create a model ramp with weight estimates we were able to calculate the spring force required to return the one-meter long ramp to the desired ten-degree angle. The ramp itself weighs in at about three hundred kilograms. Adding in a safety factor of 1.2 to compensate for any extra weight give the following equations:

$$F=x*k$$

$$350kg*1.2*9.81m/s^2=1(\sin(\theta))m*k$$

$$k=23732.9 \text{ N/m}$$

This means that the sum of all the springs required to maintain the ramps position is about 24,000 N/m. These springs will isolate the weight of the ramp from the calculations since any additional load will cause the ramp to depress and the weight of the car is the only force being added to the system.

Dividing this spring constant evenly along the ramp will ensure a sturdy result when manufactured. Another design concern for a system such as this is being certain that a concentrated load on only one are of the ramp will cause the entirety of it to depress. Not all loads will be distributed evenly along the ramp so it is critical to design it such that a point force anywhere on the ramp will cause complete depression. In order to satisfy this concern the crankshaft must stretch along the entirety of the ramp (Figure 47).

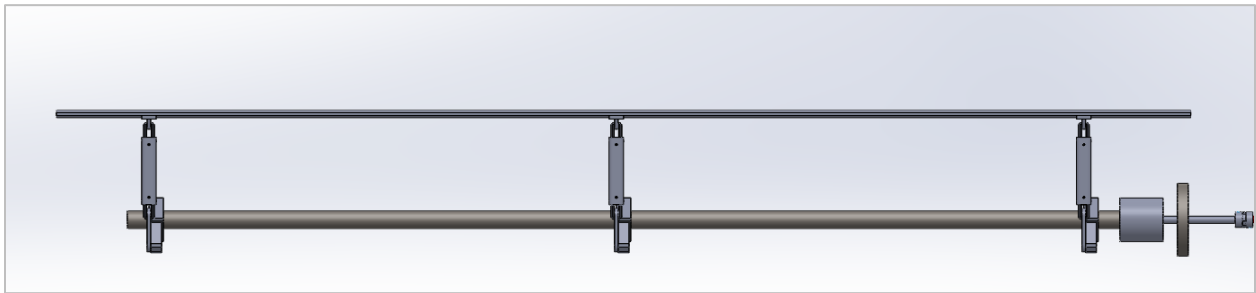


Figure 47: Full length crankshaft requirement

In the image above one can observe the ramp in a depressed state with three separate cranks attached to the main shaft below. Three cranks will create an even ramp depression since the crankshaft will pull the ramp down with it even if the load is not directly above it.

Semi-trucks are another concern for a system like this. As previously stated the range of weights traveling over this ramp is extremely large. In order to have a system that can accommodate both extremes of this spectrum of weights there needs to be a cut off point for maximum torque. This means we needed a component to the drive train that limits the torque transferred to the generator. In order to protect the system from damage due to high torques we added a torque limiter to the drivetrain similar to the one pictured in Figure 48 below.



Figure 48: Torque limiter

Once the torque limit is reached the device will disengage the crankshaft from the system so that the other components are not damaged. To allow for any vehicle to pass comfortably over this system it must also be designed with the lightest vehicles in mind. Since the springs of the system are only enough to maintain the ramp's height all of the resistance in the system will be a result of the inertia of the rotating components. For this reason we had to conduct an inertia study of the system to determine the amount of mass required for peak output via a flywheel.

To find the inertia of each individual component we first need to lay out how the drivetrain will look on the completed system. After the torque limiter there is a flywheel and a gearbox. The flywheel will contain an important component to the design of this ramp, a one way-clutch. A one-way clutch allows for the output shaft to continue to rotate after the initial input is no longer there as seen in Figure 49 below.

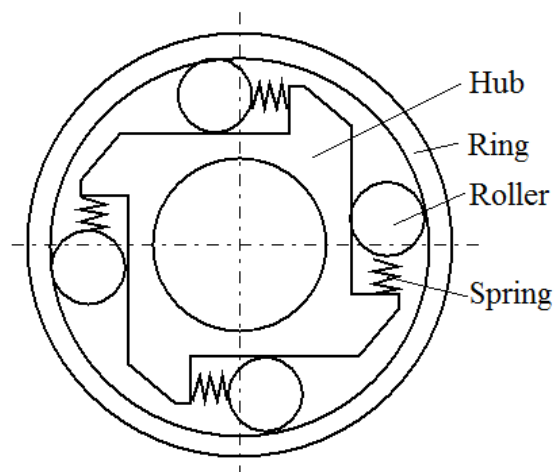


Figure 49: One-way clutch mechanism

This additional component paired with a flywheel will use the inertia of the flywheel to keep the system spinning after a car has passed. The inertia of the flywheel will make it keep rotating and the clutch will allow the wheel to rotate freely in order that one car passing will create several rotations of the generator.

Having several rotations of the main shaft is critical since it will be attached to a gearbox. A gearbox will increase the RPMs so we can spin the magnets of our generator more times to produce more energy. For this ramp design we decided to design it with a standard off the shelf 1:10 gear ratio reduction gearbox. Table 1 lists the equipment in order of the drivetrain from the ramp to the generator.

Table 1: Inertia study for full-scale ramp

Equipment		Unit Ratio	Unit Inertia (kg-m2)	Ratio to Generator	Ratio to Ramp	Inertia	
						at Generator (kg-m2)	at Ramp (kg-m2)
Ramp	I _{ramp}	1	1	10	1	0.01	1
Torque Limiter	ITL	1	0.5	10	1	0.005	0.5
Flywheel	I _{fw}	1	100.123	10	1	1.00123	100.123
Reducer	I _{red}	10	3.5	1	1	3.5	3.5
Generator	I _{gen}	1	0.256	1	0.1	0.256	0.00256
					System Inertia	4.77223	105.12556
					Max Acceptable		183.0050785
					Difference (%)		42.56
Torque limiter	4000	nm			s.f		1.740823816
Car Weight	2348.122521	kg	5200	lb			
Smallest car	300	kg					
Min Torque	511.0465869	Nm					
time	0.75	s					
alpha	2.792526803	rad/s ²					

This table shows calculations for the inertias experienced at each different components of the system. Changing these values experimentally resulted in finding that a 100 kg-m² flywheel will allow for a 300kg motorcycle to pass given the g-force requirements of our background research and still provide a 1.7 factor of safety. The governing equation for this table is as follows:

$$Inertia\ at\ generator = Inertia\ at\ crankshaft / (Ratio\ to\ generator)^2$$

The inertia for the commercial parts like the torque converter and gearbox were taken from catalogs available on different manufacturer's websites. Components that we designed were calculated using Solidworks. The crankshaft was designed with enough material to ensure it will

be strong enough to handle the max torques that are generated from semi-trucks. Below is the information used for shaft design.

Shaft design		
Max torque	58000 N*m	1.2 SF
Shear modulus	167 Mpa (MN/m²)	1.2 SF
min Radius	61 mm	

Max torque was based on an 80,000-pound vehicle traveling with a 1.2 safety factor. For a basic low carbon steel shaft we used 167 MPa as the shear modulus which was confirmed on a few different material property websites. Using the equation:

$$\tau = Tc/J$$

In this equation, “ τ ” is the maximum shear stress, “T” is the applied torque, “c” is the shaft radius, and “J” is the polar moment of inertia of the shaft. Solving with these safety factors as constrains the minimum radius of the crankshaft should be 60cm.

The entirety of the ramp has been laid out and components have been calculated. To test the concept we constructed a scaled prototype to test these calculations (Figure 50). This process began with the development of a CAD model to guide us through the manufacturing process. Below is a screenshot of a simplified CAD model for the scaled ramp model.

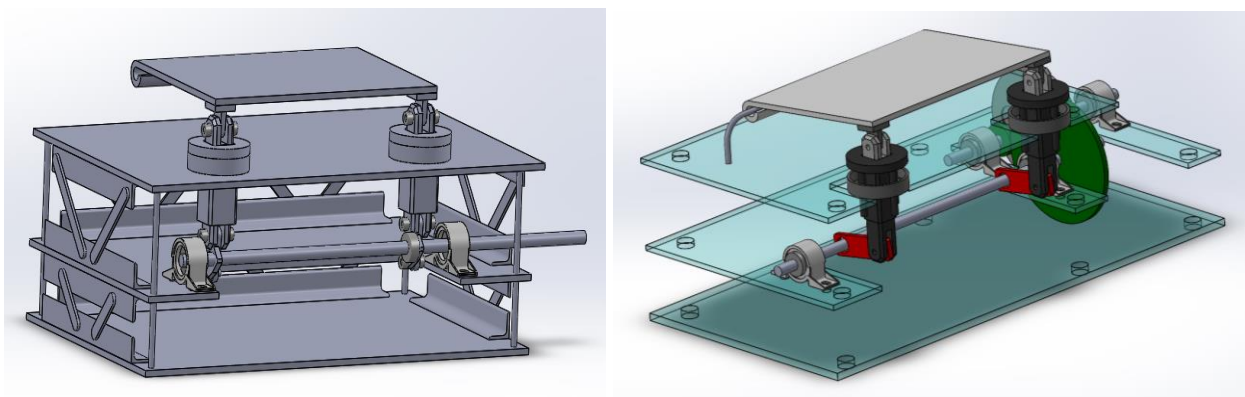


Figure 50: Simplified early CAD model (left) Final CAD model (right)

These three tiers are to house the entirety of the system and will be cut from acrylic. Since the generator discs are steel and relatively heavy to be held up by acrylic we added cross members on the sides for addition structural integrity. The picture below (Figure 51) shows the acrylic cut for the ramp itself.



Figure 51: Acrylic ramp with vinyl logo

For the ramp to function correctly an additional inertia study was conducted for this size ramp. Table 2 on the next page shows these results that we obtained from our inertia study.

Table 2: Inertia study for the prototype model ramp

						Inertia	
Equipment		Unit Ratio	Unit Inertia (kg-m ²)	Ratio to Generator	Ratio to Ramp	at Generator (kg-m ²)	at Ramp (kg-m ²)
Ramp	I _{ramp}	1	0.037	10	1	0.00037	0.037
Flywheel	I _{fw}	1	0.01	10	1	0.0001	0.01
Reducer	I _{red}	10	0.01	1	1	0.01	0.01
Generator	I _{gen}	1	0.256	1	0.1	0.256	0.00256
					System Inertia	0.26647	0.05956
					Max Acceptable		0.2711186348
					Difference (%)		78.03
					s.f		4.552025434
Smallest car	1	kg					
Min Torque	1.703488623	Nm					
time	0.5	s					
alpha	6.283185307	rad/s ²					

In the scaled prototype, the flywheel will have an inertia of about 0.01 kg-m² to allow for easy operation of the ramp with just a light motion of a wrist. This gives a very large factor of safety which results in less power out but allows for easy operation. The scaled prototype also uses the gear for its flywheel since the gear selected has the desired inertia and the location of the clutches allows for it to act as one.

4.9 Torque Estimation

Before finishing the design, it was important to estimate the torque required to turn the wheel. The first step in estimating the required torque was to estimate the torque required to spin the magnet wheel. The formula for mechanical torque is:

$$T = I * \alpha$$

Where T is the torque, I is the inertia of the object rotating, and alpha is the angular acceleration.

Another version of this equation is:

$$T = I * \frac{\omega}{t}$$

Where omega is the final angular velocity and t is the time to reach this velocity. Because we wanted to reach 120 RPM with a push or two, we found the final velocity of a 6-inch wheel rotating at 120 RPM as 0.95 m/s. The time to reach this speed was estimated to be 0.5 seconds. We calculated the inertia of our steel wheel to be 0.1 kgm². With these numbers, the estimated torque required to move the wheel alone was 0.019 Nm.

Next, we needed to estimate the torque required to move a ferromagnetic material inside the magnetic field created by the magnets. To accurately calculate this force we would need to solve Maxwell's equations. These equations involve time consuming calculations and would give us higher accuracy than we required. To save time, we estimated the force using a simpler equation. The equation:

$$F = \frac{AB^2}{2\mu_0}$$

Estimates the force on a ferromagnetic material in a constant magnetic field. In this equation A is the surface area of the object, B is the magnetic flux density acting on the object, and μ_0 is the vacuum permeability constant, equal to $4\pi * 10^{-7}$ H/m. The surface area of the steel cores is .00228 m². We found the strength of the magnetic field from the spec sheet of the magnet at ½'' away from the magnet to be 0.0857 T. For the purpose of estimation, we assumed that the strength of the field would be constant on the entire steel core. We used the distance of ½'' because with steel cores we would have the surface of the core ¼'' from the magnet and the core was ⅝'' high, so the middle would be about ½'' from the magnet. Given these parameters, the force calculated to move one of the cores through the field would be 6.656 N. For 8 coils that is 53.25 N. The centers of the cores would be 2'' or 0.0508 m from the shaft, so we would need

$53.25 * 0.04318 = 2.705 \text{ Nm}$ to get the coils to move if they had steel cores and were 0.25'' from the magnets. The attractive force between the coil wheel and the magnets was left as 0 because the wheel was far enough from the magnet that B became very low and the force was nearly 0. This estimate would be larger than an experimental value because we assumed that the field strength was constant and that each face of the cores was perpendicular to the direction of the magnetic field. The calculated value is the total torque required to start moving the coils. This value would be much larger than the torque required to keep it moving, so this value was the most important to find.

These estimates showed that the main torque to overcome in our system would be caused by the magnets. If we had no steel cores, the only torques would be the torque required to move the coil wheel in the magnetic field and the torque to overcome the inertia of the magnet wheel. Moreover, the fact that the torque on the cores was much higher raised concerns that our wheel would stop spinning as soon as we stopped pushing the ramp. If we had no cores, the system would only spin against friction, which would allow the system to get more turns from one push on the ramp.

4.9.1 Finding Torque Experimentally

From the estimates on torque, our group saw that the steel cores and magnets may have been too difficult for our ramp to move. Our group decided it best to test the actual torque values of the system. To test this, our group put the shaft with the magnet wheel on two pillow blocks. A coil wheel was put on the shaft with 4 coils attached and held in place. The coils were ¼'' from the magnets. We cut a slot into the end of the shaft and used a torque wrench with a flathead bit to rotate the system. Originally, we planned to measure torque with the torque wrench, but the wrench did not get to values below 2 Nm, which was too high. To measure the torque, we attached a spring scale to the wrench and pulled on the scale until the system turned. Knowing the distance between the scale and the shaft gave us the distance, and the scale reading showed us the force required to move the system. The test was run twice with a set of coils with steel cores and one set of 4 without cores. With the steel cores, we required 5.5 N acting on a spring scale 24 cm from the shaft, giving us 1.327 Nm of torque. Without the cores, we used 5 N acting 12 cm from the shaft, giving us 0.6 Nm of torque. So, the experimental values showed us that we would need 2.654 Nm to move 8 steel core coils and 1.2 Nm to move 8 coreless coils.

4.9.2 Removing Steel Cores

After gathering torque values, we ran another set of drill tests on the coils. The tests were run on coil wheels with 4 coils. One wheel had the steel core coils, the other wheel had coreless coils. The magnet wheel had 4 magnets 90° with alternating polarity. The cored coils were tested at 0.25" distance from the magnets. The coreless coils were put as close as they could be without any coils touching the magnets, a distance of about 0.0625". The full results are shown in Appendix F: Four Coil Drill Test. The test closest to 120 RPM for the cored coils gave a voltage of 4.24 V from 4 coils rotating at 195 RPM. The closest test for the coreless coils gave 2.88 V at 187.5 RPM. The output voltage of the coils connected in series did not show perfect sine waves. The output showed 2 positive and 2 negative peaks for each full rotation. An image can be seen in Figure 52, shown below.

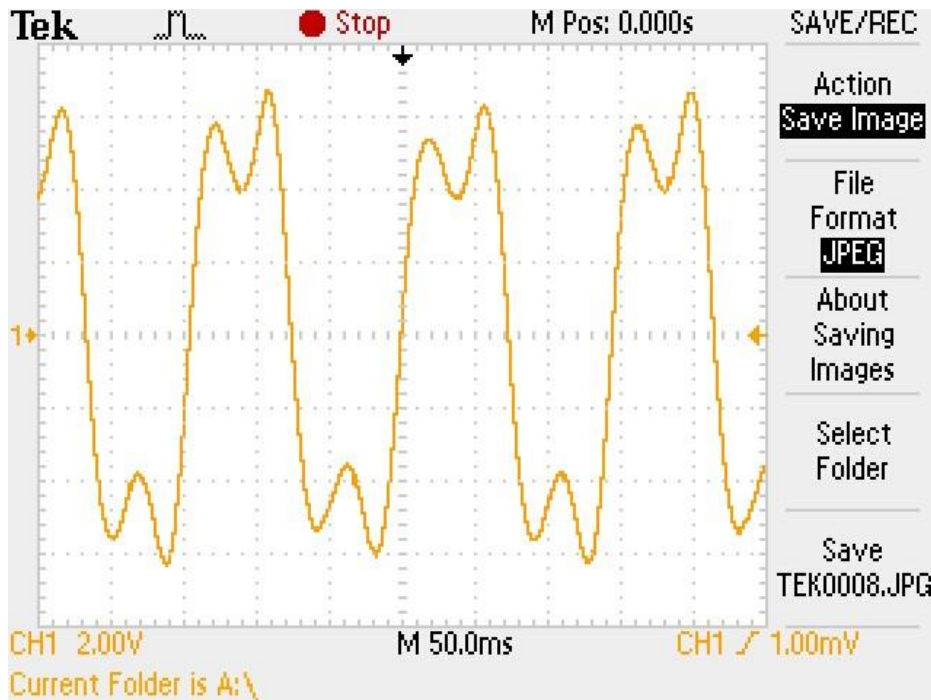


Figure 52: Output voltage of 4 coils in series

The tests showed that we could expect 68% of the voltage from cored coils from coreless coils at a closer distance. The torque required from the coreless coils was only 45.2% of the torque required from cored coils. Additionally, the coreless coils could spin freely for a time after a single impulse from the ramp, but coils with cores would stop after one quarter-turn if the ramp only gave one impulse. These data showed that removing the cores would be more effective for our push-driven prototype. For a model designed to be powered by cars, it would

make more sense to use a generator with steel cores and coils closer to the magnets because the cars would provide enough force to keep the generator running smoothly from a single impulse. After reaching this conclusion, the group removed the steel cores from the 4 coils used for testing and began constructing the output circuit designed for the coreless coils.

4.10 Ramp prototype construction

For the non-generator components, sheets of acrylic were cut on a band saw to the dimensions set from our CAD models and the three sheets were connected with threaded rod and nuts. We then added our steel crossmember for additional stability and strength by cutting the angle iron and steel flats with an angle grinder in a vice. After force fitting our magnet disc to our shaft and sliding the coil wheels in place everything was ready for testing. Figure 53 below shows the construction completed for testing.

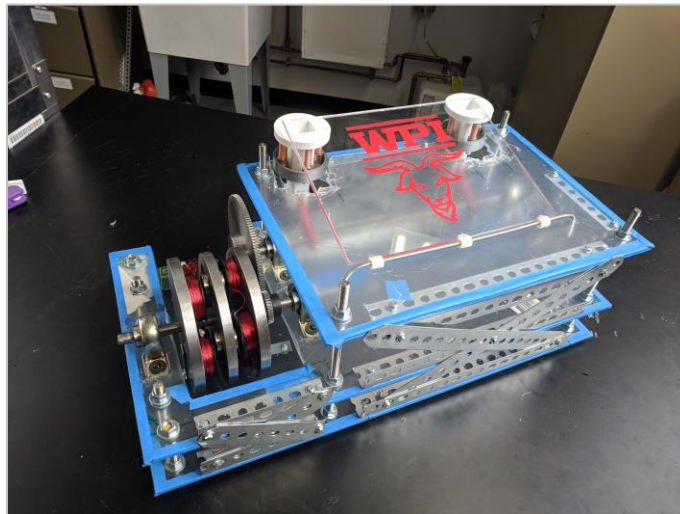


Figure 53: Completed prototype

As discussed in our design selection section, a slider crank was selected for converting the linear motion of the depressing ramp to radial motion for our generator. The components of this crank mechanism were 3D printed due to the accessibility of the printers as well as the how quickly we could create them. Since parts were so easy and quick to create we were able to tweak the design of the parts for improvements. In order to translate the motion a slider crank requires a connecting rod between the crank and slider pointed to below by the red arrow in Figure 54.

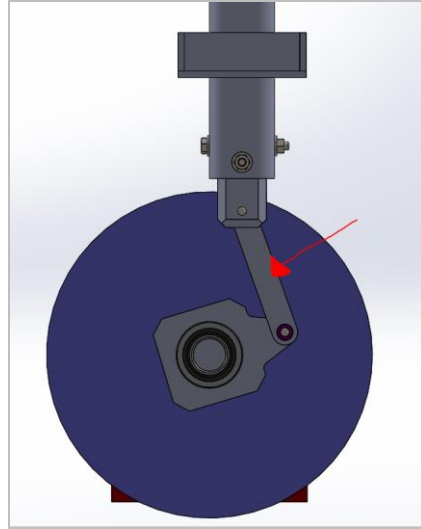


Figure 54: Connecting arm

This allows for the linear motion to continue even though the crank arm moves on a radius. However, after printing and constructing this initial design we found there were too many losses in our design and the tolerances were not tight enough for a solid slider crank. To remedy this we decided to get rid of the connecting rod and slot our crank arm. At this point we also realized that the losses were not properly accounted for in our torque calculations so the torque arm would also need to be lengthened to accommodate. Another change that had to be made was with the springs. Since the torque required increased we decided to change the slider to have poles pass through cup underneath to avoid any buckling as seen below.

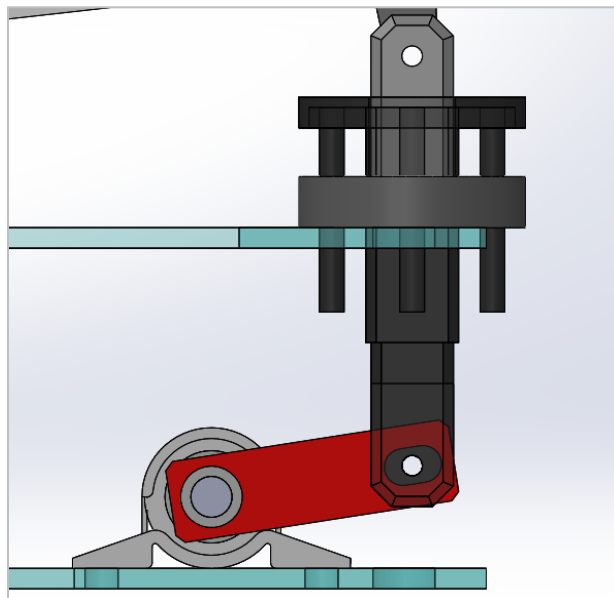


Figure 55: New slider crank

In Figure 55 one can see the now increased and slotted torque arm which will still allow for the mechanism to work as well as the anti-buckling poles for the springs. Another improvement made to the initial construction was to add bushings for these spring poles. The 3D printed parts had a lot of friction so adding some brass bushings to the design helped reduce this and also allowed for more control over the tolerances which resulted in a sturdier mechanism.

Chapter 5. Results

Once the improvements to the ramp were finished, we assembled the generator, attached it to the ramp, and tested the output of the full prototype. To test the output, we pushed the ramp repeatedly to spin the wheel for a few seconds. The output from the generator was connected to an oscilloscope and measured. Two pictures of the output from the oscilloscope is shown below in Figure 56. The pictures are of the same waveform, with the right photograph on a shorter time scale to show the output in greater detail.

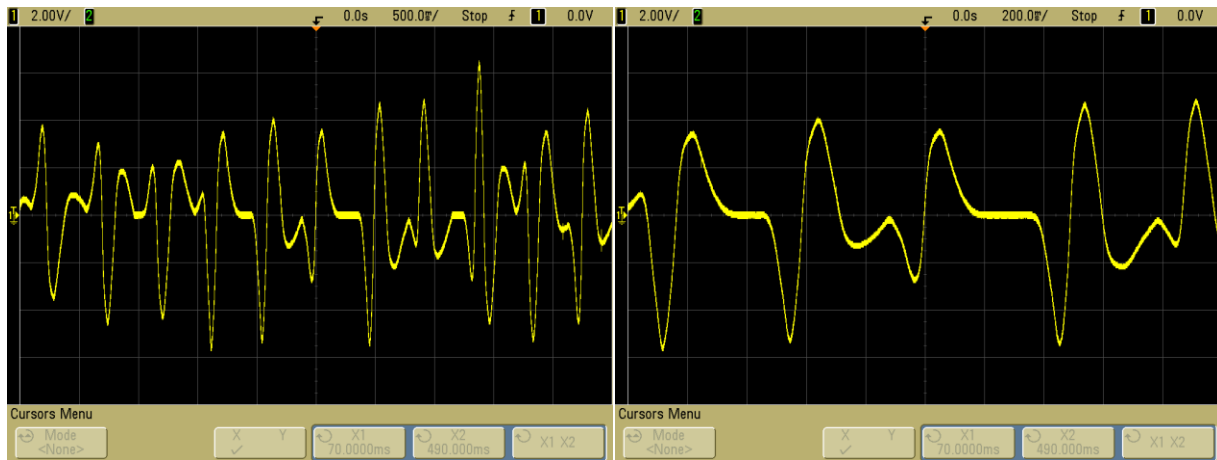


Figure 56: Output from generator powered by hand

The output consists of sine waves of varying frequency. The frequency changing is due to the way the generator is spun. After someone pushes the ramp, the generator spins for about 0.5 seconds. As generator slows, the frequency of the output slows. The next push speeds up the generator again, creating a varying frequency. The peak voltages ranged from a maximum of 6.2 V to a minimum of 2.1 V. Most waveforms tended to have peaks from 4.2 V to 3 V. The root mean squared (RMS) voltage for sine waves with these peaks is from 2.97 V to 2.12 V.

Our prototype behaved closely to our expectations. The peak voltage values within 4.2 V and 3 V were close to our estimate of 3.776 peak voltage out for the circuit. Our group measured the rotation of the generator using a tachometer, and the generator spun at a peak of 150 RPM right after the ramp was pushed; above our estimate of 120 RPM. On weaker pushes, the ramp spun at speeds ranging from 90 RPM to 131 RPM.

After we made sure the prototype was behaving properly, we assembled the output circuit and attached it to the output of the generator. For the circuit we used the schematic described in

section 4.7 with 21 LEDs rather than 4. The system powered half of the LEDs at a time, with each half alternating with the other as the ramp was pushed. Very weak pushes failed to power the LEDs, and single pushes only powered the LEDs as long as the generator spun, about 0.5 seconds. This behavior was normal, because the LEDs were set up such that half of the LEDs were powered by the positive portion of the AC output, and the other half were powered by the negative portion. The LEDs did not stay on after the generator stopped spinning because a charging capacitor cannot be used with an AC waveform.

To test the efficiency of the system, we connected the output of the generator to a 51 Ω resistor. We ran the system with a drill and measured the power used by the drill with a plug power meter. The drill used 43 W to run when it was running on its own at around 480 RPM. When connected to our system, the drill used 47 W while running at the same speed. This means that the power into our system was roughly 4 W. To calculate the output power, we measured the voltage across the resistor as the drill was running. The output waveform can be seen below, in Figure 57.

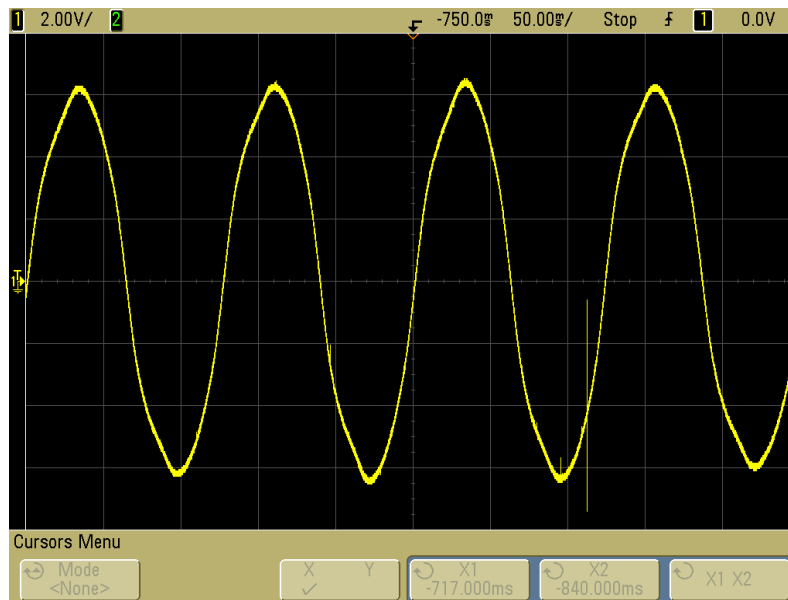


Figure 57: Voltage across resistor when drill powered

These measurements were taken with a different oscilloscope than previous tests. The output showed a normal sine wave without the irregular peaks from previous tests. The output showed peak voltages of 6.25 V. Converting from peak to RMS for sine waves is simply $V_{rms} = V_{pk}/\sqrt{2}$, giving us an RMS voltage to the resistor of 4.42 V. The output power is the total voltage V_t . To find the total voltage, we need to account for the voltage lost in the wiring for the coils.

The resistance of the 8 coils was measured with a multimeter to be 11.1Ω . With this we can find the total voltage by treating the system as a voltage divider:

$$V_t = V_r(R_r R_r + R_c)$$

Where V_t is the total RMS voltage, V_r is the RMS voltage of the resistor, R_r is the resistance of the resistor, and R_c is the resistance of the coils. With the given parameters, we measured an output voltage of 5.38 V. The current is this total voltage divided by the total resistance, giving us 86.7 mA. The output power is this current times the total voltage, resulting in 0.466 W. Dividing this value by the input power of 4 W gives us an efficiency of 11.66%. The low efficiency of the generator is mostly because the coils in the generator were coreless. If the generators had cores, the majority of the force we put on the system would be used to overcome the magnetic forces acting on the cores and overcoming the inertia of the steel wheel holding the magnets would be a small portion of the force. Because we have no cores, most of the force on our system is used to overcome the inertia of the steel wheel, and the magnetic forces between the magnets and the wheels are only a small portion of the total energy used. This reduces our efficiency, because most of our input power is going to inertia, rather than to the coils.

Once we finished testing the output circuit on a breadboard, we soldered the circuit on perfboard and soldered the generator to it. The circuit can be seen below in Figure 58.

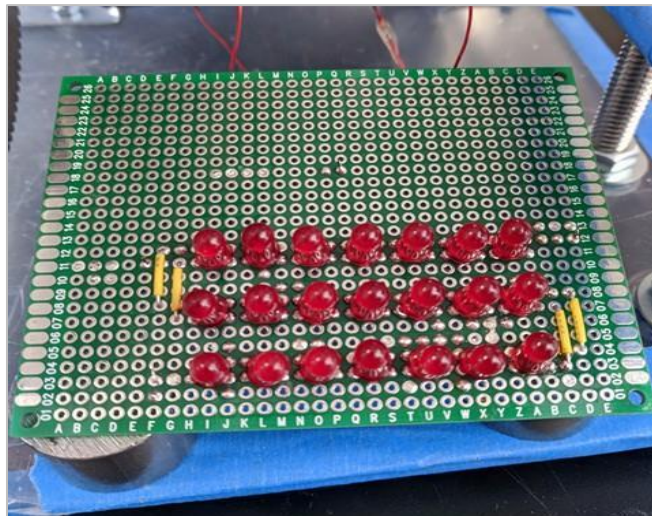


Figure 58: Output circuit of generator

Chapter 6. Conclusions

We created a working prototype to demonstrate our idea for a system that can both harvest energy from braking vehicles and reduce the vehicle's need to brake. Using a slider crank mechanism with one-way clutches produced a ramp that always returns to its initial position and can be actuated once and allow for several turns of the output shaft. Our generator provided enough power for an array of LEDs to be illuminated however, the overall output of the system is low. Since this scaled prototype required us to remove the steel cores from our coils the output was severely reduced. One possibility to improve the output is to have a larger gear ratio since the torque required is lower after knocking the cores out.

The next step for this project would be to build and test a full scaled prototype. Having vehicles actuate the system will provide increased torque which will allow for the steel cores to remain in the coils resulting in better results than our coreless coils in the scaled version.

If this project were to be continued some aspects that could be reviewed further would be adding a transmission to the system. One of the major drawbacks of this ramp is that you must design the loads for the lightest weight vehicle classes, motorcycles. If there were a mechanism for detecting the weight of the oncoming vehicle and could engage/disengage a series of flywheels one could yield far better outputs on average. This would also allow for the removal of the torque limiter, which makes the current design act as if every vehicle that passes over it is just a lightweight vehicle.

One other consideration that must be made is the materials selected for the ramp's surface itself. We would recommend in the future to have a civil engineer to review material selections to ensure minimal wear to the system itself and the rubber of car tires.

References

1. Allain, Rhett. (2015). Tested: How Bright LEDs Are Compared to Other Lights. Retrieved on October 3, 2017, from <https://www.wired.com/2015/06/tested-bright-leds-compared-lights/>
2. Bartholomew, Edward. Powelka, Aimee. (2013). LED Street Lights, What is Your Plan?. Retrieved on October 4, 2017, from <http://www.mass.gov/eea/docs/doer/green-communities/pubs-reports/led-street-lighting-slides-09-11-13.pdf>
3. Boston Region Metropolitan Planning Organization. (n.d.). Average Daily Traffic on Massachusetts Roads. Retrieved on September 28, 2017, from <http://www.ctps.org/geoserver/www/apps/adtApp/index.html>
4. Brooks M., Turner H.M., Inductance of coils, University of Illinois Engineering Experiment Station Bulletin, no. 53, 1912.
5. Central Massachusetts Regional Planning Commission. (2014). Central Massachusetts Regional Traffic Flow. Retrieved September 28, 2017, from <http://cmrpc.org/sites/default/files/Documents/Trans/Maps/2012RegionalTrafficFlow8.5x11.pdf>
6. City of Des Moines Engineering. (n.d.). Why Can't Speed Bumps Be Used On All Streets to Slow Traffic? Retrieved August 30, 2017, from http://www.dmgov.org/departments/engineering/pdf/faq9_speed_bumps_and_humps.pdf
7. Clarke R. (2010). An Introduction to the air cored coil. Retrieved on December 1, 2017 from http://info.ee.surrey.ac.uk/Workshop/advice/coils/air_coils.html
8. Digi-Key European Editors (2012). Energy-Efficient LED Street Lights Improve Visibility, Safety. Retrieved on October 4, 2017, from <https://www.digikey.com/en/articles/techzone/2012/may/energyefficient-led-street-lights-improve-visibility-safety>
9. Dmitriev, Victor. Electric Power Generating Speed Bump. Victor Dmitriev, assignee. Patent US 2013/0193692 A1. 1 Aug. 2013. Print.
10. Eisele R. (2017). Calculate the intersection area of two circles. Retrieved on December 2, 2017 from <https://www.xarg.org/2016/07/calculate-the-intersection-area-of-two-circles/>

11. ElectricRate. (2017). Massachusetts Residential Electric Rates. Retrieved on October 4, 2017, from <http://www.electricrate.com/residential-rates-massachusetts/>
12. Empowering Pumps. (2017). AC Induction Motors vs. Permanent Magnet Synchronous Motors. Retrieved on October 4, 2017, from <http://empoweringpumps.com/ac-induction-motors-versus-permanent-magnet-synchronous-motors-fuji/>
13. Grotton, Jacob., Schramm, Christopher., Poss, Kaitlin., Evangelakos, William. (2016). Harvesting Wasted Vehicular Kinetic Energy from Transportation Infrastructure. Retrieved on August 15, 2017, from <https://web.wpi.edu/Pubs/E-project/Available/E-project-042816-111324/>
14. Hanson, Peter. (2017). Why You Need To Know “How Much Does A Motorcycle Weigh?” Retrieved on September 29, 2017, from <http://letsridemotorbike.com/how-much-does-a-motorcycle-weigh/>
15. Hyperphysics. (n.d.) Faraday’s Law. Retrieved on September 27, 2017 from <http://hyperphysics.phy-astr.gsu.edu/hbase/electric/farlaw.html>
16. Juang, Yi., Li, Shuo. (2001). Measuring and Analyzing Vehicle Position and Speed Data at Work Zones Using Global Positioning System. Retrieved September 20, 2017, from https://www.workzonesafety.org/files/documents/database_documents/00587.pdf
17. K&J Magnetics (n.d.). Steel Thickness Calculator. Retrieved on November 28, 2017, from <https://www.kjmagnetics.com/thickness.calculator.asp>
18. Kour R, Charif A (2016). Piezoelectric Roads: Energy Harvesting Method Using Piezoelectric Technology. *Innov Ener Res* 5:132. Retrieved August 29, 2017, from <https://www.omicsonline.org/open-access/piezoelectric-roads-energy-harvesting-method-using-piezoelectrictechnology-ier-1000132.php?aid=73891>
19. Kuphaldt T. (n.d.). Permeability and Saturation. Retrieved on November 28, 2017, from <https://www.allaboutcircuits.com/textbook/direct-current/chpt-14/permeability-and-saturation/>
20. Lean Engineering. (n.d.). How Does an Alternator Work? Retrieved on October 2, 2017, from <http://www.learnengineering.org/2014/04/working-of-alternator.html>
21. Maurya, Akhilesh., Bokare, Prashant. (2012). Study of Deceleration Behaviour of Different Vehicle Types. Retrieved September 15, 2017, from [http://ijtte.com/uploads/2012-10-01/5ebd8343-9b9c-b1d4IJTTE%20vol2%20no3%20\(7\).pdf](http://ijtte.com/uploads/2012-10-01/5ebd8343-9b9c-b1d4IJTTE%20vol2%20no3%20(7).pdf)

22. Meyboudi S. (2013). The Feasibility of Communication Among Pumps in a District Heating System. Retrieved on December 12, 2017, from https://www.researchgate.net/figure/260658571_fig11_Fig-12-Dimensions-of-a-multilayer-coil-with-rectangular-cross-section
23. Miller-Wilson, Kate. (2014). List of Car Weights. Retrieved August 22, 2017, from http://cars.lovetoknow.com/List_of_Car_Weights
24. MIT Science Writing and New Media. (2010). Final Report on Jerkling an Energy-saving Speed Bump. Retrieved August 30, 2017, from https://ocw.mit.edu/courses/comparative-media-studies-writing/21w-732-science-writing-and-new-media-fall-2010/projects/MIT21W_732F10_jerklingrep.pdf
25. North Central Texas Council of Governments. (2014). Vehicle Types - Descriptions and Photos. Retrieved September 20 2017, from <http://www.nctcog.org/trans/air/programs/fleet/policy/calculator/type.asp>
26. U.S. Department of Transportation. (2013). Annual Vehicle Distance Traveled in Miles and Related Data. Retrieved on September 28, 2017, from <https://www.fhwa.dot.gov/policyinformation/statistics/2013/vm1.cfm>
27. Zyga, Lisa. (June 2009). Passing cars to generate energy for new UK supermarket. Retrieved on September 26, 2017, from <https://phys.org/news/2009-06-cars-energy-uk-supermarket.html>

Appendix A: Car Weights

Model	Curb Weight
-------	-------------

2012 Toyota Camry	3,190 pounds
2012 Toyota Prius	3,042 pounds
2012 Toyota Avalon	3,572 pounds
2013 Toyota Matrix	2,888 pounds
2013 Chevrolet Equinox LS	3,777 pounds
2013 Chevrolet Corvette	3,208 pounds
2013 Chevrolet Malibu	3,393 pounds
2012 Chrysler Town and Country	4,652 pounds
2012 Subaru Outback	3,495 pounds
2014 Subaru Impreza	3,208 pounds
2013 BMW 740i Sedan	4,344 pounds
2012 Honda Civic LX Coupe	2,617 pounds
2012 Cadillac Escalade EXT	5,949 pounds
2012 MINI Cooper Hatchback	2,535 pounds
2013 Dodge Durango	4,756 pounds
2013 Hyundai Accent	2,396 pounds
2013 Hyundai Elantra	2,701 pounds

2012 Scion xB	3,084 pounds
2012 Scion TC	3,102 pounds
2013 Buick Regal	3,600 pounds
2014 Buick LaCrosse	3,756 pounds
2014 Buick Verano	3,300 pounds
2013 Kia Optima Hybrid	3,496 pounds
2014 Kia Cadenza	3,668 pounds
2012 Lexus IS-F	3,780 pounds
2013 Audi A6	3,682 pounds
2014 BMW 5-Series	3,814 pounds
2012 Nissan Cube	2,768 pounds
2012 Nissan Maxima	3,540 pounds
2014 Nissan Versa	2,354 pounds
2013 Ford Focus	2,935 pounds
2013 Ford Taurus	4,037 pounds
2012 Smart Fortwo	1,808 pounds
2013 Mazda MAZDA6	3,323 pounds
2014 Porsche Panamera	3,968 pounds

Appendix B: MATLAB Code

```
function [] = dynamic_ramp_remake(c, theta, m, vin, mu, k)
% c is length of ramp, theta is angle of ramp in degrees
% m is mass in kg, vin is initial velocity in m/s
% mu is ramp friction, k is the spring constant of the ramp's spring

b = c*sind(theta); % b is height of the ramp
g = 9.81; % g is acceleration due to gravity

db = b; % db is instantaneous height of ramp (this is the initial value)
dTheta = theta; % dTheta is instantaneous theta (this is initial)
dh = 0; % instantaneous height of car

% dc is the instantaneous position along the ramp
for dc = .01:.01:c
    db2 = b - ((m*g*dc)./(k*c*.985)); % calculate db at this point
    % check for cases where db is negative
    if db2 < 0
        db2 = 0;
    end

    dTheta2 = asind(db2./c); % calculate dTheta at this point
    dh2 = dc*sind(dTheta2);

    db = [db db2];
    dTheta = [dTheta dTheta2];
    dh = [dh dh2];
end

% loop through dh to get velocity values
```

```

length_dh = length(dh);
dc = 0:.01:c;
disp(length(dc))
disp(length(dh))
dv = vin; % dv is instantaneous velocity
for x = 2:1:length_dh
    if dTheta(x) == 0
        dv2 = ((dv(x-1).^2)+(2*g*dh(x))-(2*g*mu*.01)).^5;
    else
        dv2 = ((vin.^2)+(2*g*dh(x))-((2*g*mu*dh(x))./tand(dTheta(x))))).^5;
    end
    dv = [dv dv2];
end

time = [0]; % set time array, initial is 0

% Find time based on position along c
for dc=.01:.01:c;
    n = int16(dc*100);
    aTerm = (g./2)*sin(dTheta(n));
    bTerm = dv(n);
    cTerm = -dc;
    poly = [aTerm bTerm cTerm];
    if min(roots(poly)) < time(n)
        time2 = max(roots(poly));
    else
        time2 = min(roots(poly));
    end
    time = [time time2];
end

```

```
dc = 0:0.01:c; % define dc to allow graphing
```

```
plot(time, dv)  
xlabel('Time in s')  
ylabel('Velocity in m/s')
```

```
figure()  
plot(time, dc)  
xlabel('Time in s')  
ylabel('Position along ramp in m')
```

```
figure()  
plot(time, dh)  
xlabel('Time in s')  
ylabel('Height of car in m')
```

```
figure()  
plot(time, db)  
xlabel('Time in s')  
ylabel('Height of end of ramp in m')  
end
```

Appendix C: Pendulum test results

Test I				
Trial	Vmax (volts)	t (ms)	Speed (m/s)	RPM
0	0.228	126	0.261	32.7
1	0.268	100	0.33	41
2	0.6	52	0.635	79.2
3	0.64	48	0.688	86.2
4	0.328	109	0.303	37.95
5	0.244	127	0.26	32.57
6	0.3	110	0.3	37.58
7	0.7	50	0.66	82.67
8	0.536	57	0.579	72.53
9	0.56	56	0.589	73.78
10	0.312	109	0.303	37.95
11	0.336	90	0.367	45.97
12	0.324	88	0.375	46.97
13	0.576	58	0.567	71.02
14	0.55	63	0.524	65.64
15	0.352	69	0.478	59.87
16	0.328	80	0.413	51.73
17	0.5	44	0.75	93.95
18	0.536	44	0.75	93.95
19	0.456	53	0.623	78.04

Test II				
Trial	Vmax (volts)	t (ms)	Speed (m/s)	RPM
0	1.1	51.2	0.645	80.79
1	0.624	88	0.375	46.97
2	0.96	55	0.6	75.16
3	1.42	39.6	0.833	104.34
4	0.88	63.6	0.519	65.01
5	0.96	71	0.465	58.25
6	1.2	51	0.647	81.04
7	1.08	53	0.623	78.04
8	0.76	79	0.418	52.36
9	0.608	94	0.351	43.97

Appendix D: Intersection calculator code

```
#include <stdlib.h>
#include <stdio.h>
#include <getopt.h>
#include <string.h>
#include <unistd.h>
#include <math.h>

#define M_PI 3.14159265358979323846
#define MIN(x, y) (((x) < (y)) ? (x) : (y))
#define MAX(x, y) (((x) > (y)) ? (x) : (y))

int main(int argc, char **argv)
{
    double getArea(double Ar, double Ax, double Ay, double Br, double Bx, double
By)
    {
        // do intersection calculation math
        double d = hypot(Bx - Ax, By - Ay);
        // only do this math if they are intersecting
        if (d < Ar + Br) {
            double a = Ar*Ar;
            double b = Br*Br;
            double c = sqrt((Ax-Bx)*(Ax-Bx) + (Ay-By)*(Ay-By));
            double phi = (acos((b+(c*c)-a) / (2*Br*c)))*2;
            double theta = (acos((a+(c*c)-b) / (2*Ar*c)))*2;
            double area1 = 0.5*theta*a - 0.5*a*sin(theta);
            double area2 = 0.5*phi*b - 0.5*b*sin(phi);

            if (d < fabs(Ar - Br)) { // handle cases where one circle is within the other
                double area = M_PI * MIN(a, b);
                return area;
            }

            return area1 + area2;
        }
        return 0;
    }

    // get input from command line
    double Ar, Ax, Ay, Br, Bx, By;
    char x;
    while((x = getopt(argc, argv, "Y:y:R:r:X:x:")) != -1) // get input
    switch(x) {
```

```

    case 'Y':
        Ay = atof(optarg);
        break;
    case 'y':
        By = atof(optarg);
        break;
    case 'R':
        Ar = atof(optarg);
        break;
    case 'r':
        Br = atof(optarg);
        break;
    case 'X':
        Ax = atof(optarg);
        break;
    case 'x':
        Bx = atof(optarg);
        break;
}
// open an output file for the csv
FILE *file;
file = fopen("output.csv", "w"); // open file

if (file == NULL) {
    printf("Error, file not made properly");
    return 1;
}

// loop through distance between circles' centers (start at max, end at 0)
double distance;
double division = .000542;
double timePerDivision = .001;
double lastArea = 0;
double diffArea;
double area = 0;
double time = 0;
Ax = 0; // make one circle stay at 0, edit other circle;
Ay = 0;
By = 0; // assume same height
for (distance = Ar + Br; distance >= -(Ar + Br + division); distance -= division) {
    Bx = distance; // update 2nd circle
    area = getArea(Ar, Ax, Ay, Br, Bx, By);
    diffArea = (area - lastArea) / timePerDivision;
    //if (diffArea != 0) {
    fprintf(file, "%f, %f, %f \n", time, area, diffArea);
    //}
}

```



```
        // update variables
        time += timePerDivision;
        lastArea = area;
    //    if (By == 0) {
    //        By += division;
    //    } else {
    //        By -= division;
    //    }
    }

    if (!(file == NULL)) {
        fclose(file);
    }

    printf("Diff: %f\n", fabs(Ar-Br));
    printf("TEST: %f\n", Ar+Br);
    printf("Output written to output.csv \n");
    return 0;
}
```

Appendix E: Single Coil Drill Test

Steel Core 1/4" Test			Steel Core 1/8" Test			Coreless 1/8" Test	
RPM	Peak Voltage (V)		RPM	Peak Voltage (V)		RPM	Peak Voltage (V)
280	1.92		80	0.92		31	0.14
96	0.56		130	1.52		75	0.3
116	0.72		170	1.84		128	0.472
50	0.44		258	2.6		194	0.728
167	1		379	3.56		238	0.88
220	1.36					375	1.4
384	2.36						

Appendix F: Four Coil Drill Test

4 Steel Core Coils Drill Test			4 Coreless Coils Drill Test	
RPM	Peak Voltage (V)		RPM	Peak Voltage (V)
195	4.24		187.5	2.88
329	6.16		268	4.32
681	11.6		435	7.2